

Supporting Information for

**Improved Catalytic Performance by Changing Surface and Textural
Properties of Ru Supported Bifunctional Periodic Mesoporous
Organosilicas in the Aerobic Oxidation of Alcohols**

Omid Pourshiani,^a Babak Karimi,^{*a,b} Hesamodin Moradi,^a Werner R. Thiel,^c Hojatollah Vali,^d
Pietro Mastrorilli,^e and Stefano Todisco^e

^a *Department of Chemistry, Institute for Advanced Studies in Basic Sciences (IASBS), Zanjan, 45137-66731, Iran*

^b *Research Center for Basic Sciences & Modern Technologies (RBST), Institute for Advanced Studies in Basic Sciences (IASBS), Zanjan 45137-66731, Iran*

^c *Fachbereich Chemie, RPTU Kaiserslautern-Landau, Erwin-Schrödinger-Str. 54, 67663 Kaiserslautern, Germany*

^d *Department of Anatomy and Cell Biology and Facility for Electron Microscopy Research, McGill University, Montreal, Quebec, H3A 2A7, Canada*

^e *DICATECh, Politecnico di Bari, Bari, I-70125 Italy*

Table of Contents

General Information	5
Material	5
Synthesis of 1,3-bis(trimethoxysilylpropyl)imidazolium chloride (BTMSPCI).....	5
Synthesis of BFPMO Materials.....	6
Preparation of Ru@U-Ph15 Catalyst	7
General Procedure for the Oxidation of Alcohols	7
General Procedure for the Recyclability of Ru@U-Ph15 in the Aerobic Oxidation of Benzyl alcohol.....	8
References	42
Table S1. Ru loading of Ru@BFPMOs obtained by ICP-AES	18
Table S2. Comparison of several Ru-based catalytic systems in the oxidation of alcohols into the corresponding carbonyl compounds	27
Scheme S1. Synthesis of 1,3-bis(trimethoxysilylpropyl) imidazolium chloride (BTMSPCI)	6
Figure S1. Nitrogen adsorption-desorption isotherms of the BFPMO materials	9
Figure S2. BJH-Plots of the BFPMO materials.....	9
Figure S3. Nitrogen adsorption-desorption isotherms of the BFPMO (U-Ph15), Ru@U-Ph15 and Re-Ru@U-Ph15 materials.....	10
Figure S4. BJH-Plots of the BFPMO (U-Ph15), Ru@U-Ph15 and Re-Ru@U-Ph15 materials.....	10
Figure S5. FTIR spectra of the BFPMO materials	10
Figure S6. ¹³ C and ²⁹ Si CP/MAS NMR spectra of a) Ph-15- and b) Et-15-BFPMO.....	11
Figure S7. Thermogravimetric analysis curve of the BFPMO (U-Et15) material under the nitrogen atmosphere	12
Figure S8. Thermogravimetric analysis curve of the BFPMO (P-Et15) material under the nitrogen atmosphere.....	12
Figure S9. Thermogravimetric analysis curve of the BFPMO (U-Ph15) material under the nitrogen atmosphere	13
Figure S10. Thermogravimetric analysis curve of the BFPMO (P-Ph15) material under the nitrogen atmosphere	13
Figure S 11. Thermogravimetric analysis curve of the BFPMO (U-Et15) material under the oxygen atmosphere	14
Figure S12. Thermogravimetric analysis curve of the BFPMO (P-Et15) material under the oxygen atmosphere.....	14
Figure S13. Thermogravimetric analysis curve of the BFPMO (U-Ph15) material under the oxygen atmosphere	15
Figure S14. Thermogravimetric analysis curve of the BFPMO (P-Ph15) material under the oxygen atmosphere	15
Figure S15. Thermogravimetric analysis curve of the Ru@U-Ph15 material under the nitrogen atmosphere ...	16
Figure S16. Thermogravimetric analysis curve of the Ru@U-Ph15 material under the oxygen atmosphere.....	16
Figure S17. Thermogravimetric analysis curve of the recovered Ru@U-Ph15 material under the nitrogen atmosphere	17
Figure S18. Thermogravimetric analysis curve of the recovered Ru@U-Ph15 material under the oxygen atmosphere	17
Figure S19. SEM image of the Ru@U-Ph15 (scale bar: 200 nm).	18
Figure S20. SEM image of the Ru@U-Ph15 (scale bar: 500 nm).	19
Figure S21. EDX Elemental mapping of (a) Nitrogen and (b) Ruthenium of the Ru@U-Ph15 Catalyst	19
Figure S23. HRTEM image of the Unplugged Ph-BFPMO (scale bar: 100 nm).	20
Figure S24. HRTEM image of the Unplugged Ph-BFPMO with 2D hexagonal structure and uniform cylindrical mesochannels (scale bar: 5 nm).	20
Figure S25. HRTEM image of the Ru@U-Ph15 (scale bar: 100 nm).....	21
Figure S26. HRTEM image of the Ru@U-Ph15 (scale bar: 50 nm).....	21
Figure S27. HRTEM image of the Ru@U-Ph15 (scale bar: 20 nm).....	22
Figure S28. Energy-dispersive X-ray spectroscopy (EDS) of Ru@U-Ph15.....	22
Figure S29. XPS survey spectrum of Ru@U-Ph15.....	23
Figure S30. High-resolution XPS spectrum of Ru3p of Ru@U-Ph15.....	23
Figure S31. High-resolution XPS spectrum of N1s of Ru@U-Ph15	24
Figure S32. High-resolution XPS spectrum of O1s of Ru@U-Ph15	24
Figure S33. High-resolution XPS spectrum of C1s of Ru@U-Ph15	24

Figure S34. XPS survey spectrum of Re-Ru@U-Ph15	25
Figure S35. High-resolution XPS spectrum of Ru3p of Re-Ru@U-Ph15	25
Figure S36. HRTEM image of the Re-Ru@U-Ph15 (scale bar: 50 nm).	26
Figure S37. HRTEM image of the Re-Ru@U-Ph15 (scale bar: 10 nm).	26
Figure S38. Gas chromatogram of benzyl alcohol reaction (Table 4, Entry 1)	28
Figure S39. Gas chromatogram of 4-methoxybenzyl alcohol reaction (Table 4, Entry 2).....	28
Figure S40. Gas chromatogram of 4-methylbenzyl alcohol reaction (Table 4, Entry 3).....	28
Figure S41. Gas chromatogram of 4-methylbenzyl alcohol (blank)	29
Figure S42. Gas chromatogram of 4-isopropylbenzyl alcohol reaction (Table 4, Entry 4)	29
Figure S43. Gas chromatogram of 4-isopropylbenzyl alcohol (blank).....	29
Figure S44. Gas chromatogram of 4-chlorobenzyl alcohol reaction (Table 4, Entry 5).....	30
Figure S45. Gas chromatogram of 4-chlorobenzyl alcohol (blank)	30
Figure S46. Gas chromatogram of 4-bromobenzyl alcohol reaction (Table 4, Entry 6)	30
Figure S47. Gas chromatogram of 4-nitrobenzyl alcohol reaction (Table 4, Entry 7)	31
Figure S48. Gas chromatogram of 4-nitrobenzyl alcohol (blank).....	31
Figure S49. Gas chromatogram of 3-nitrobenzyl alcohol reaction (Table 4, Entry 8)	31
Figure S50. Gas chromatogram of 3-chlorobenzyl alcohol reaction (Table 4, Entry 9).....	32
Figure S51. Gas chromatogram of 3-methoxybenzyl alcohol reaction (Table 4, Entry 10).....	32
Figure S52. Gas chromatogram of 3-methoxybenzyl alcohol (blank)	32
Figure S53. Gas chromatogram of 2,4-dichlorobenzyl alcohol reaction (Table 4, Entry 11).....	33
Figure S54. Gas chromatogram of 2,6-dichlorobenzyl alcohol reaction (Table 4, Entry 12).....	33
Figure S55. Gas chromatogram of 2-nitrobenzyl alcohol reaction (Table 4, Entry 13)	33
Figure S56. Gas chromatogram of 2-nitrobenzyl alcohol (blank).....	34
Figure S57. Gas chromatogram of 2-methylbenzyl alcohol reaction (Table 4, Entry 14).....	34
Figure S58. Gas chromatogram of 2-methylbenzyl alcohol (blank)	34
Figure S59. Gas chromatogram of 1-naphthyl methanol reaction (Table 4, Entry 15)	35
Figure S60. Gas chromatogram of 3-pyridine methanol reaction (Table 4, Entry 16)	35
Figure S61. Gas chromatogram of 2-furyl alcohol reaction (Table 4, Entry 17)	35
Figure S62. Gas chromatogram of 5-hydroxymethylfurfural (HMF) reaction (Table 4, Entry 18).....	36
Figure S63. Gas chromatogram of cinnamyl alcohol reaction (Table 4, Entry 19)	36
Figure S64. Gas chromatogram of 2-cyclohexene-1-ol reaction (Table 4, Entry 20).....	36
Figure S65. Gas chromatogram of diphenylmethanol reaction (Table 4, Entry 21).....	37
Figure S66. Gas chromatogram of diphenylmethanol (blank)	37
Figure S67. Gas chromatogram of 1-phenyl-1-ethanol reaction (Table 4 Entry 22)	37
Figure S68. Gas chromatogram of 1-phenyl-1-propanol reaction (Table 4, Entry 23)	38
Figure S69. Gas chromatogram of cyclooctanol reaction (Table 4, Entry 24).....	38
Figure S70. Gas chromatogram of cycloheptanol reaction (Table 4, Entry 25).....	38
Figure S71. Gas chromatogram of cyclohexanol reaction (Table 4, Entry 26)	39
Figure S72. Gas chromatogram of cyclohexanone (blank).....	39
Figure S73. Gas chromatogram of cyclohexanol (blank).....	39
Figure S74. Gas chromatogram of borneol reaction (Table 4, Entry 27).....	40
Figure S75. Gas chromatogram of 2-heptanol reaction (Table 4, Entry 28).....	40
Figure S76. Gas chromatogram of 2-octanol reaction (Table 4, Entry 29)	40
Figure S77. Gas chromatogram of 3-phenyl-1-propanol reaction (Table 4, Entry 30)	41
Figure S78. Gas chromatogram of 1-heptanol reaction (Table 4, Entry 31).....	41
Figure S79. Gas chromatogram of 1-octanol reaction (Table 4, Entry 32)	41

Materials and Methods

General Information

The transmission electron microscopy (TEM) images were taken on FEI Tecnai Spirit microscope operated at an accelerating voltage of 150 kV. Textural properties were obtained using a Belsorp analyser (BELMAX, Japan) at 77 K. The samples were degassed at 373 K for 5 h, prior to the N₂ adsorption-desorption analysis. Specific surface areas were evaluated from the relative pressure range of 0.05-0.15 by Brunauer–Emmett–Teller (BET) method. Pore size distribution (PSD) of the samples was calculated from the adsorption branch using the Barrett–Joyner–Halenda (BJH) method. Total pore volumes were determined using the adsorbed volume at $P/P_0 \approx 0.995$. Solid-state magic-angle spinning (MAS) nuclear magnetic resonance (NMR) spectra were collected on a Bruker 400 MHz Avance FT-NMR spectrometer with the MAS speed of 13 kHz. Cross-polarization (CP) technique was used for both ¹³C and ²⁹Si spectra, which were referenced to tetramethylsilane. XPS spectra of the samples were recorded on the Kratos Analytical X-ray photoelectron spectrometer. Thermogravimetric analysis was performed using a NETZSCH STA 409 PC/PG instrument (Germany) at scan rates of 10 K.min⁻¹ from 25 to 800 °C under both N₂ and O₂ atmospheres. The nitrogen content of the materials was determined using elemental analysis (C, H, N) by the Vario-EL CHNS instrument. The fourier transform infrared (FTIR) spectra of the prepared BFPMOs were recorded on a Bruker-Vector 22 FTIR spectrometer in the range of 400 and 4000 cm⁻¹, and the samples were prepared by the KBr pellet method. The oxidation products were analyzed using a Varian CP-3800 gas chromatograph (GC) equipped with a capillary column [Teknokroma Meta. BLOOD 2 (30 m × 0.53 mm × 2.0 μm)] and a flame-ionization detector (FID).

Materials

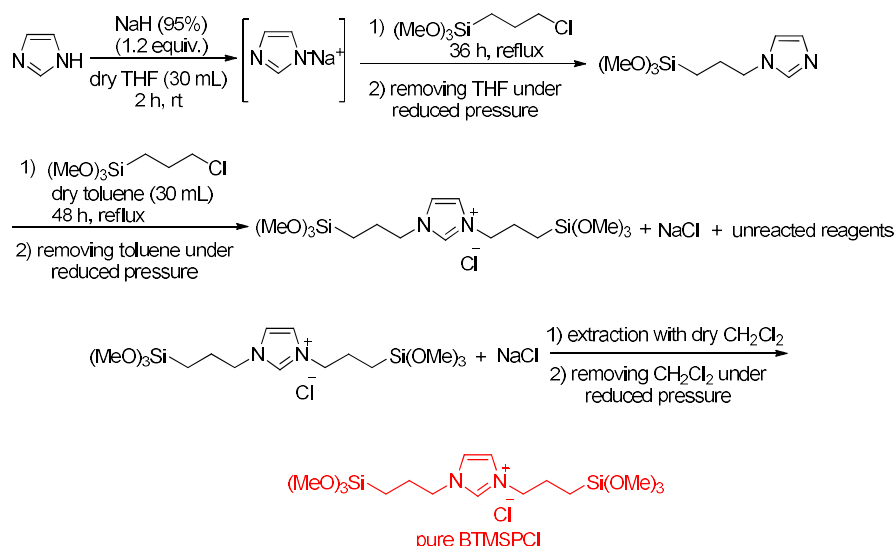
Sodium hydride (NaH 95%), Pluronic P123 (EO₂₀PO₇₀EO₂₀ (EO = ethylene oxide, PO = propylene oxide), average $M_n = 5800$) 1,4-bis(triethoxysilyl)benzene (BTEB), 1,4-bis(trimethoxysilyl)ethane (BTME), and tetramethoxyorthosilicate (TMOS) were purchased from Sigma-Aldrich Company. Potassium perruthenate (KRuO₄), imidazole and (3-chloropropyl)trimethoxysilane (CPTMS) were purchased from Acros Company. Potassium chloride (KCl) and conc. HCl (37%) were obtained from Merck Company. Imidazole was recrystallized in distilled CH₂Cl₂ and dried under vacuum for 3 days at room temperature. All the reagents were used without further purification.

Synthesis of 1,3-bis(trimethoxysilylpropyl)imidazolium chloride (BTMSPCI)

The ionic liquid precursor (BTMSPCI) was prepared according to the procedure used in our previous reports.^{1, 2} Typically, a suspension of sodium imidazolide in dry THF was prepared through the direct reaction of freshly dried imidazole (2 g) and NaH 95% (0.77 g) in a flame-dried two-neck flask containing dry THF (60 mL) under an argon atmosphere. CPTMS (5.4 mL) was added to the above suspension and the resulting mixture was refluxed for 30 h. The reaction mixture was allowed to cool at room temperature and then the solvent was removed under a reduced pressure condition until an oily mixture containing NaCl was obtained. In the second part, (3-chloropropyl)trimethoxysilane (5.4 mL) and dry toluene (60 mL) were added to the oily mixture, and then the reaction flask was placed under the reflux condition for 48 h. The toluene phase was separated from the resulting two-phasic mixture, and then dry CH₂Cl₂ (60 mL) was added into the flask to take out the precipitated NaCl. In the next step, the CH₂Cl₂ phase was transferred to the well-dried two-neck flask, and volatiles were removed under reduced pressure. Finally, the ionic liquid (BTMSPCI) was

washed with dry toluene (5×50 mL) to remove the unreacted starting materials and obtain pure BTMSPCI.

^1H NMR (CDCl_3 , 400 MHz): δ = 0.47 (br, 4H) 1.84 (m, 4H) 3.37 (s, 18H), 4.21 (br, 4H), 7.41 (s, 2H), 10.46 (s, 1H). ^{13}C NMR (CDCl_3 , 100 MHz): δ = 5.8, 24.0, 50.5, 51.5, 122.0, 137.1. Hz).



Scheme S1. Synthesis of 1,3-bis(trimethoxysilylpropyl) imidazolium chloride (BTMSPCI)

Synthesis of BFPMO Materials

The plugged BFPMO materials (comprising 15% phenylene or ethylene bridge and 10% ionic liquid) were synthesized according to the procedure previously reported in our research group.¹ In a typical method, the Pluronic P123 (2.0 g) template was dissolved in a solution of H_2O (12.20 g) and HCl (2 M, 49.53 g). After three hours, KCl (10.23 g) was added to the reaction flask, and the mixture was kept under stirring until a homogenous solution was obtained. A pre-mixture of TMOS (15.00 mmol, 2.65 g), BTMSPCI (2.00 mmol, 1.0 g) and the organic bridge (BTEB (3.00 mmol, 1.40 g) or BTME (3.00 mmol, 0.943 g)) in dry methanol was added to the obtained solution, and then the reaction was stirred at $40\text{ }^\circ\text{C}$ for 24 h. The resulting mixture was heated under static condition at $100\text{ }^\circ\text{C}$ for 72 h. The obtained white solid was collected by vacuum filtration and then washed with a solution of ethanol and

conc. HCl (100:3 volume ratios) using a Soxhlet apparatus for 48 h to remove the surfactant. Finally, the BFPMO product was dried at 60 °C overnight.

For the synthesis of unplugged BFPMO materials, the organosilica and silica precursors were added to the reaction flask in two steps; so that in the first step, BTMSPCl and BTEB (or BTME) were added to the reaction flask, and the resulting mixture was stirred for at least 15 minutes. In the second step, TMOS was added to the mixture, and stirring was continued at 40 °C for 24 h. The structure of these materials was thoroughly characterized using various analyses.

Preparation of Ru@U-Ph15 Catalyst

For the preparation of the Ru@U-Ph15 catalyst, the unplugged BFPMO material containing phenyl and imidazolium bridges (0.5 g, 0.464 mmol.g⁻¹ ILs) was dispersed in deionized water (10 mL) and sonicated for at least 30 min. Then, KRuO₄ (0.016 g, 0.08 mmol), dissolved in deionized water (20 mL), was slowly added to the above suspension and vigorously stirred at room temperature for 24 h. Finally, the suspension was filtered and washed with deionized water (3×10 mL) and acetone (2×10 mL). The resulting gray powder was dried in an oven at 70 °C overnight. The exact loading amount of Ru species was calculated by ICP-AES analysis (0.192 mmol.g⁻¹).

General Procedure for the Oxidation of Alcohols

In a 5 mL two-necked round-bottom flask equipped with a magnetic stir bar and condenser alcohol substrate (0.25 mmol), **Ru@U-Ph-15 (19.5 mg, 1.5 mol% of Ru)** and toluene (1 mL) were added. The top of condenser was sealed tightly with a rubber septum. The reaction vessel was evacuated and re-filled three times with oxygen and finally a balloon filled with

pure oxygen (622 torr) was attached to the top of condenser. The reaction mixture was stirred at 90 °C for the indicated reaction time (see Table 5 of the manuscript). After completion of the reaction, **the catalyst was separated by centrifugation** and the catalyst was washed several times with toluene and ethyl acetate to ensure the extraction of any substrate and corresponding product that may be trapped into the channels of the catalyst. The reaction solution was then filtered using a 0.45 µm syringe filter (Sartorius Minisart RC,) and analyzed by GC without any further purification.

General Procedure for the Recyclability of Ru@U-Ph15 in the Aerobic Oxidation of Benzyl alcohol

To a test tube equipped with a condenser, **benzyl alcohol (108 mg, 1mmol), Ru@U-Ph-15 (78 mg, 1.5 mol% of Ru)** and toluene (4 mL) were added. Top of the condenser was sealed tightly with a rubber septum. The reaction vessel was evacuated three times and refilled with oxygen and finally a balloon filled with pure oxygen (622 torr) was attached to the top of the condenser. The reaction mixture was stirred at 90 °C for 3 hours. The yield of the reaction was evaluated by GC analysis. The Ru@U-Ph15 catalyst was then **separated by centrifugation**, washed several times with toluene and ethyl acetate, and dried in an oven at 70 °C. For the next runs, the recovered catalyst was weighed and appropriate amounts of benzyl alcohol and toluene (proportionate to the above amounts) were added to the test tube. The oxidation reactions for the next cycles were repeated following the same procedure as described above. The reaction time for all cycles was **3 hours, which was the optimal time for complete oxidation of benzyl alcohol to benzaldehyde according to the data in Table 4** in the manuscript.

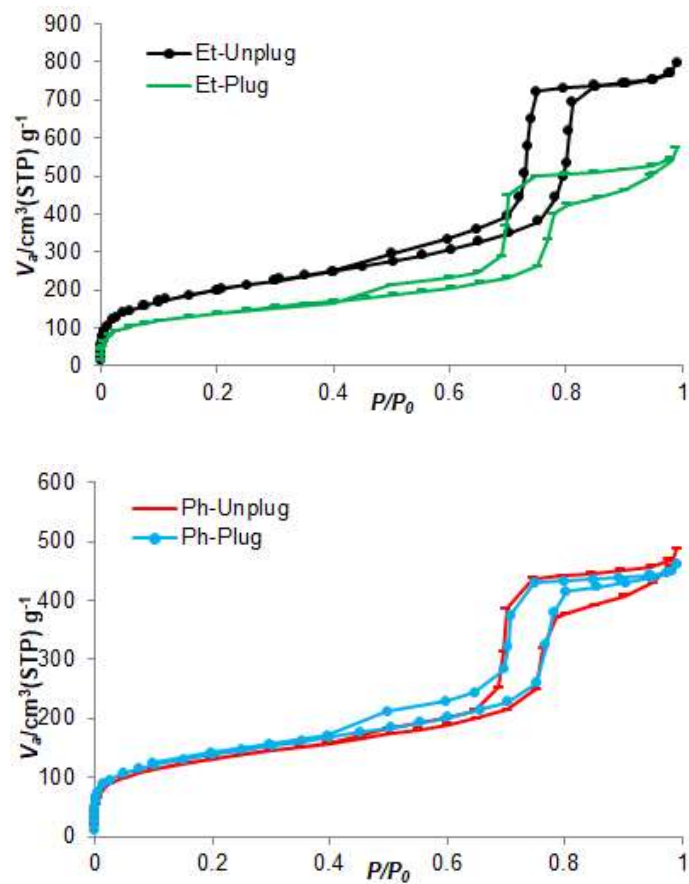


Figure S1. Nitrogen adsorption-desorption isotherms of the BFPMO materials

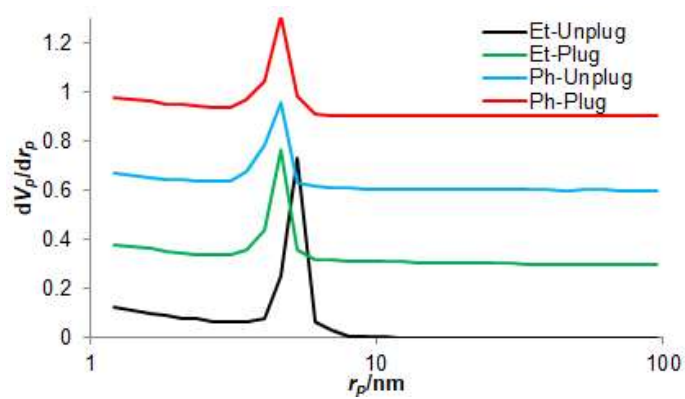


Figure S2. BJH-Plots of the BFPMO materials

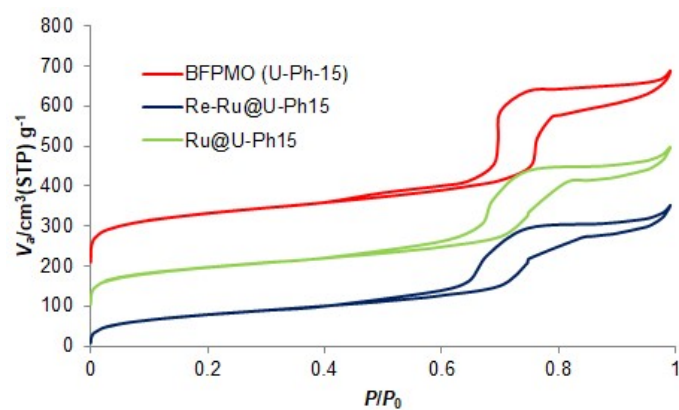


Figure S3. Nitrogen adsorption-desorption isotherms of the BFPMO (U-Ph15), Ru@U-Ph15 and Re-Ru@U-Ph15 materials

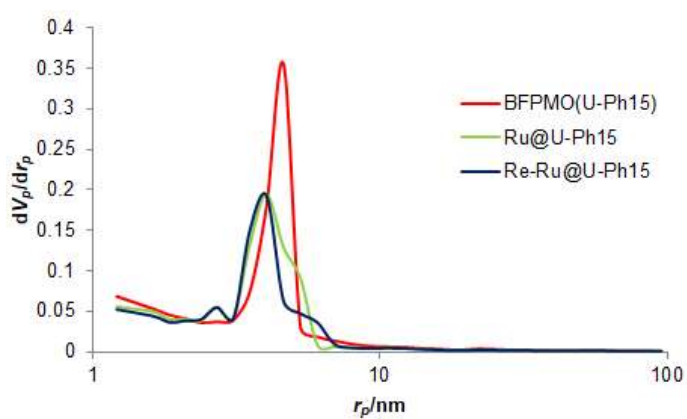


Figure S4. BJH-Plots of the BFPMO (U-Ph15), Ru@U-Ph15 and Re-Ru@U-Ph15 materials

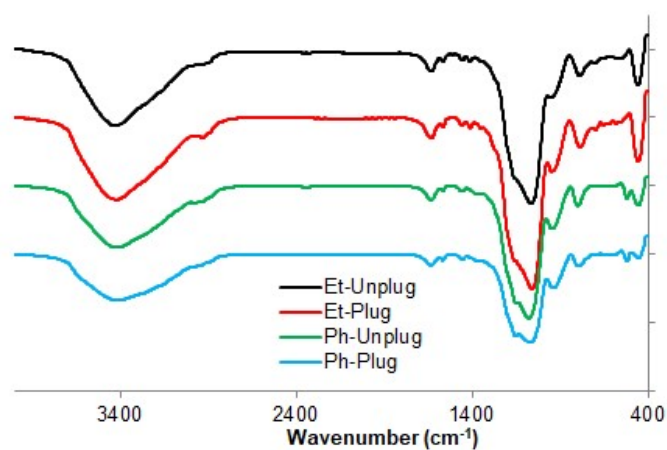


Figure S5. FTIR spectra of the BFPMO materials

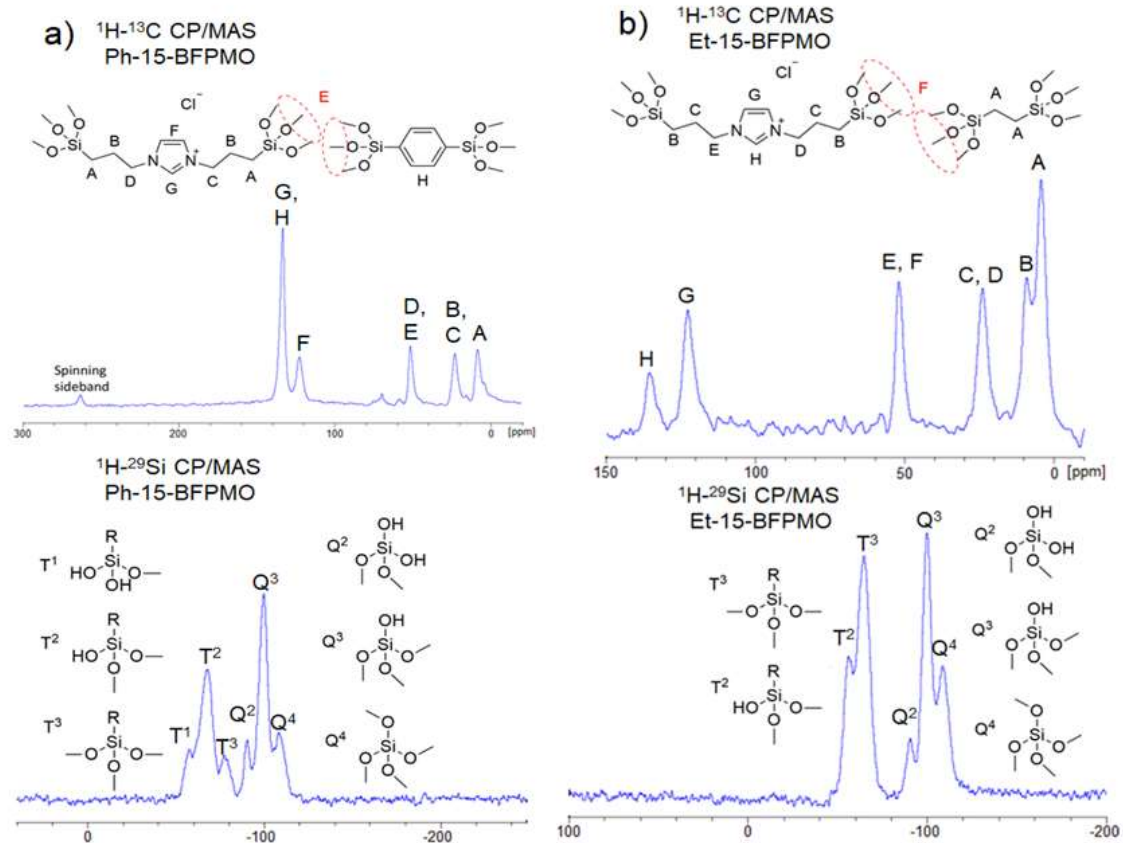


Figure S6. ^{13}C and ^{29}Si CP/MAS NMR spectra of a) Ph-15- and b) Et-15-BFPMO

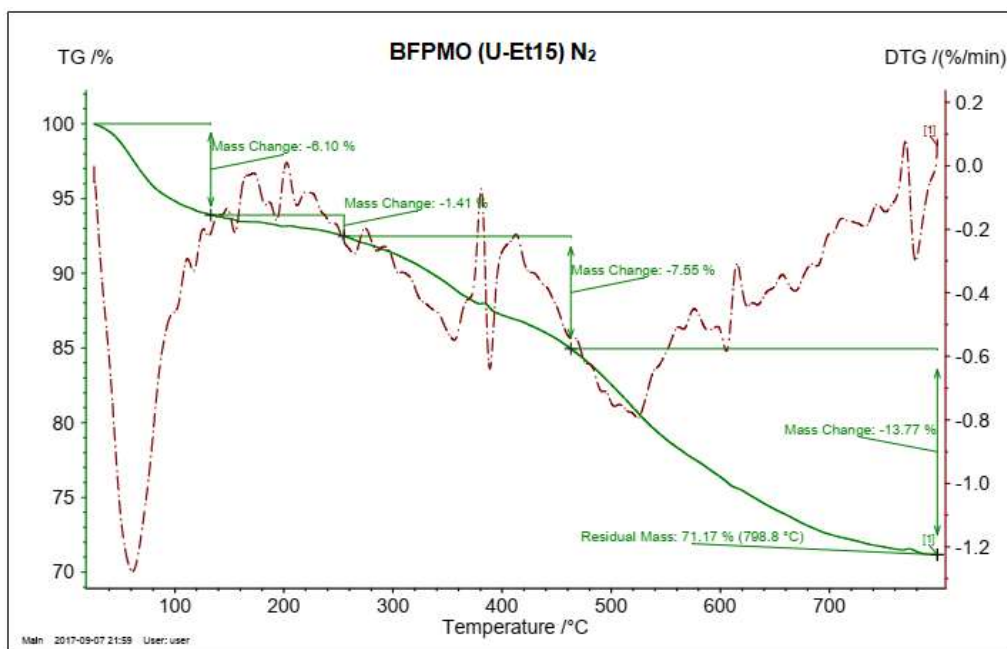


Figure S7. Thermogravimetric analysis curve of the BFPMO (U-Et15) material under the nitrogen atmosphere

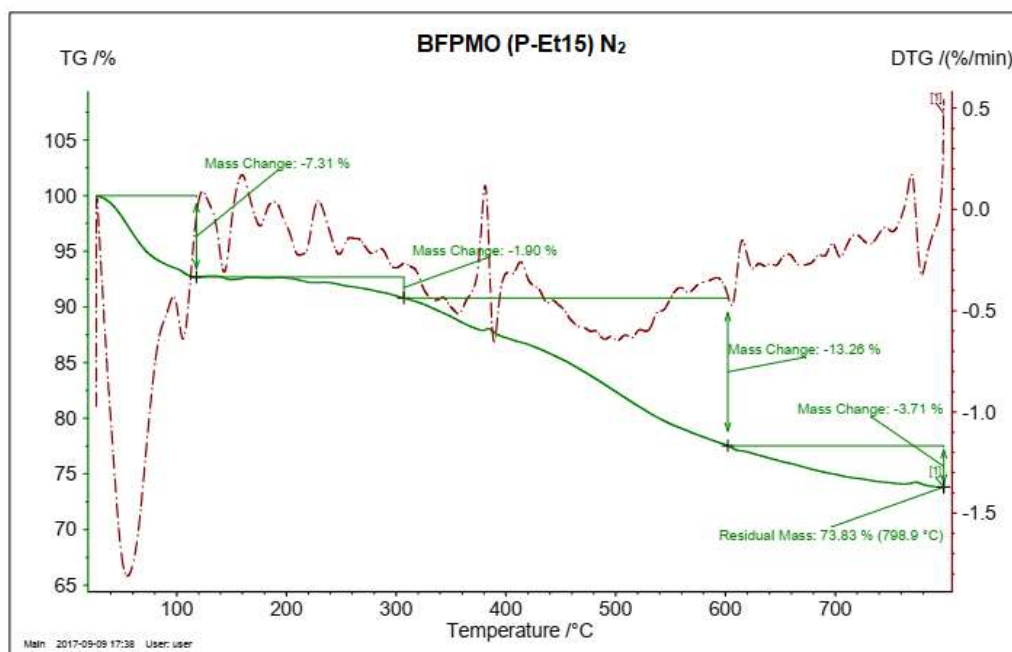


Figure S8. Thermogravimetric analysis curve of the BFPMO (P-Et15) material under the nitrogen atmosphere

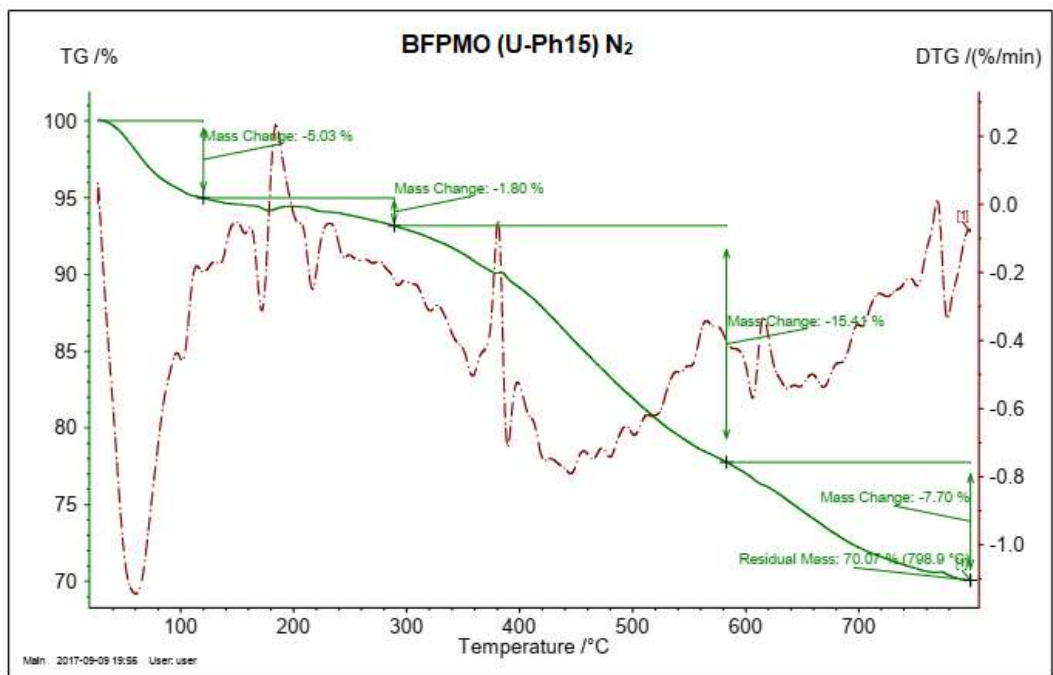


Figure S9. Thermogravimetric analysis curve of the BFPMO (U-Ph15) material under the nitrogen atmosphere

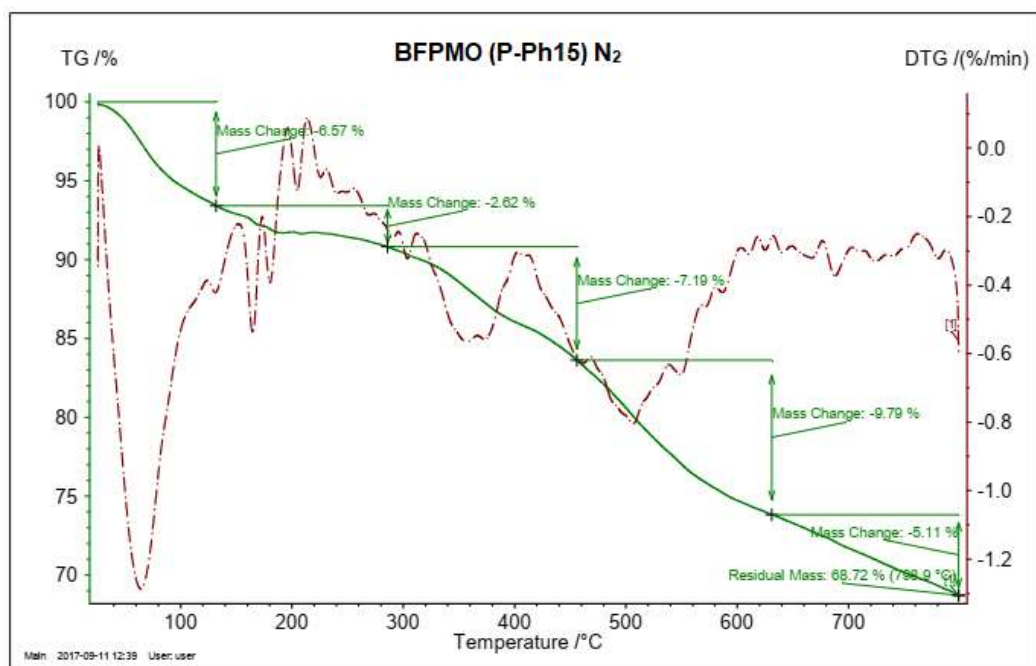


Figure S10. Thermogravimetric analysis curve of the BFPMO (P-Ph15) material under the nitrogen atmosphere

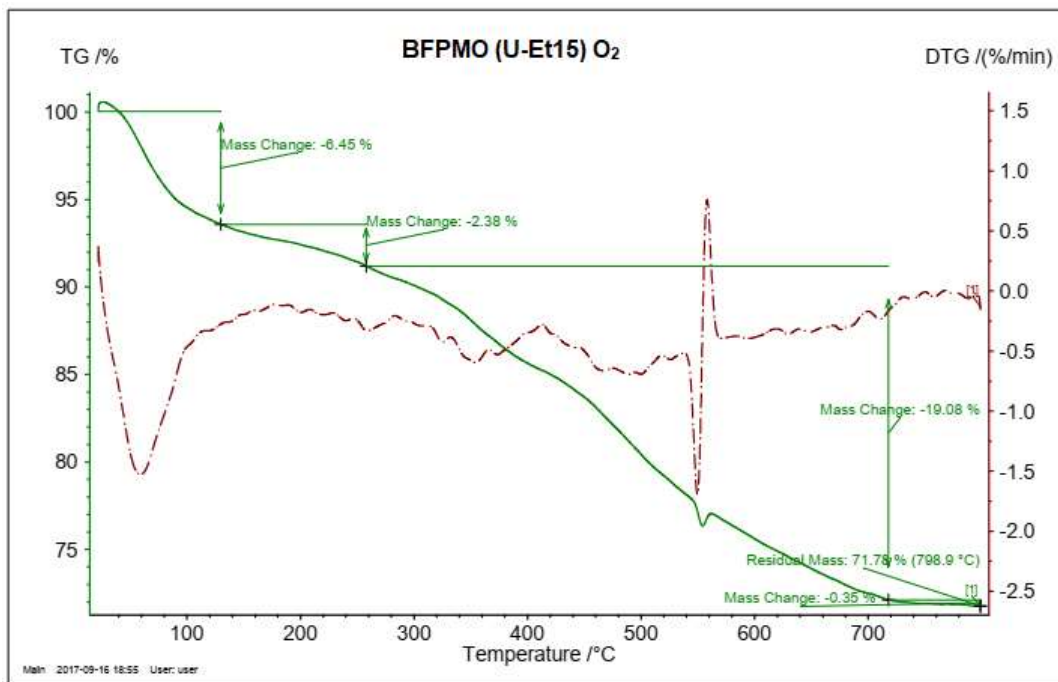


Figure S 11. Thermogravimetric analysis curve of the BFPMO (U-Et15) material under the oxygen atmosphere

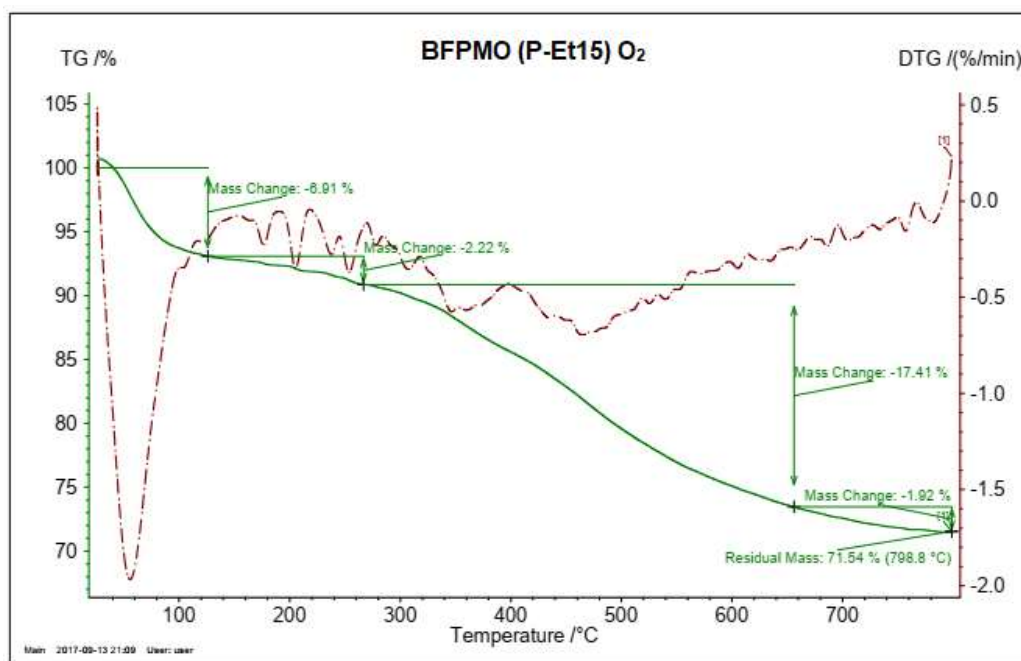


Figure S12. Thermogravimetric analysis curve of the BFPMO (P-Et15) material under the oxygen atmosphere

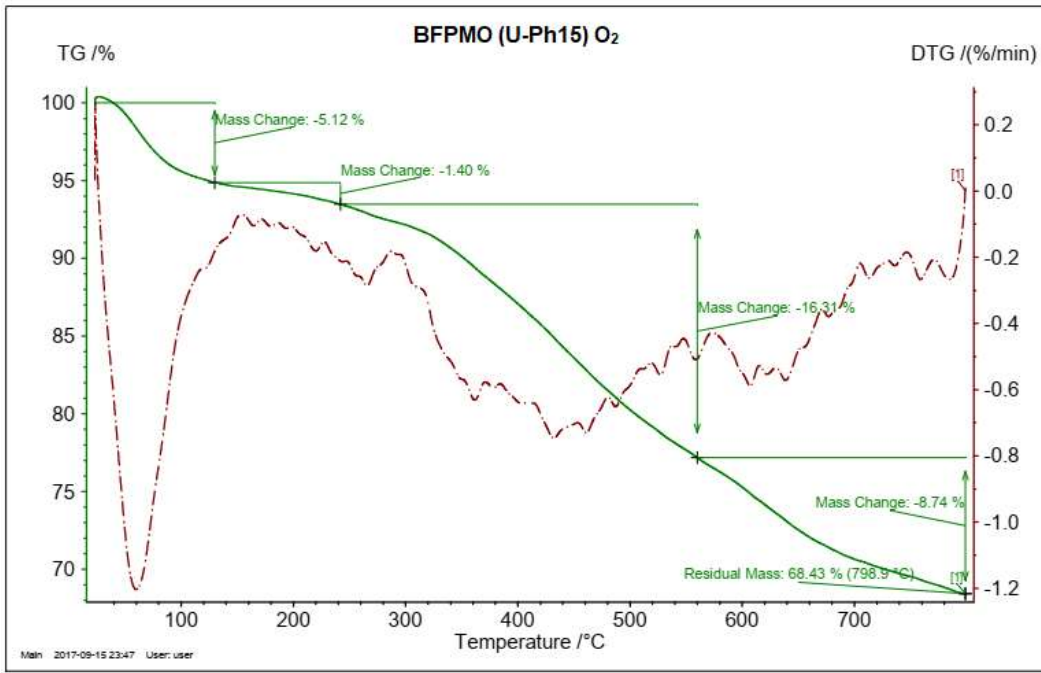


Figure S13. Thermogravimetric analysis curve of the BFPMO (U-Ph15) material under the oxygen atmosphere

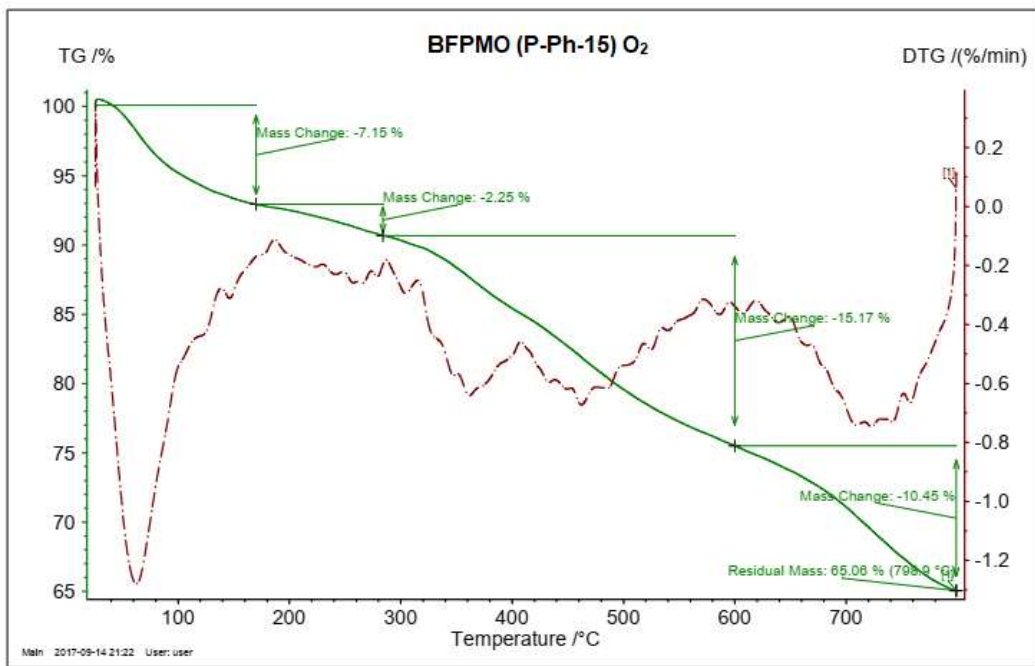


Figure S14. Thermogravimetric analysis curve of the BFPMO (P-Ph15) material under the oxygen atmosphere

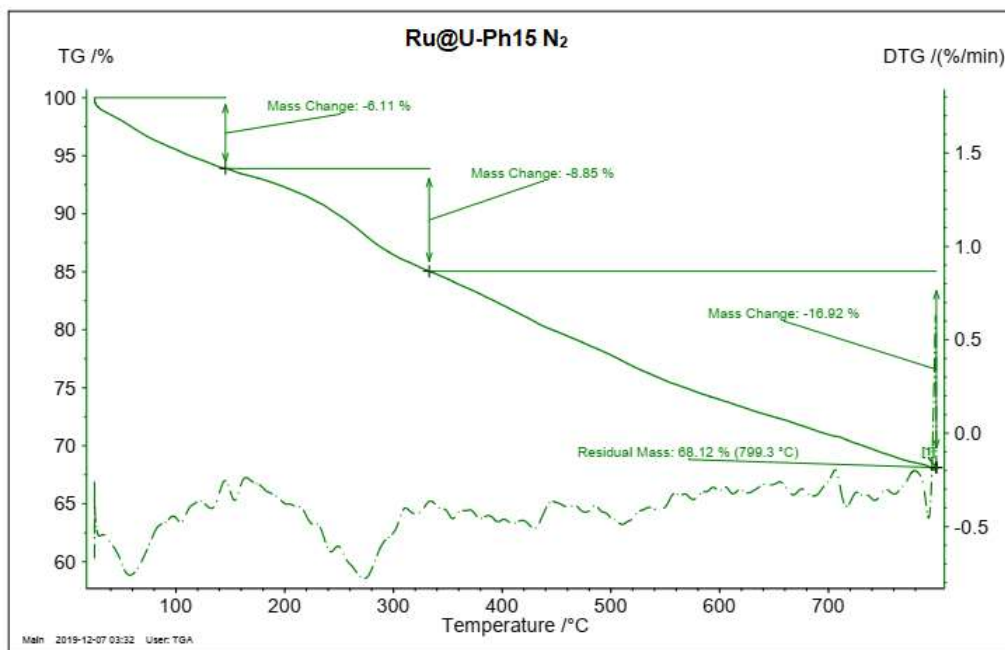


Figure S15. Thermogravimetric analysis curve of the Ru@U-Ph15 material under the nitrogen atmosphere

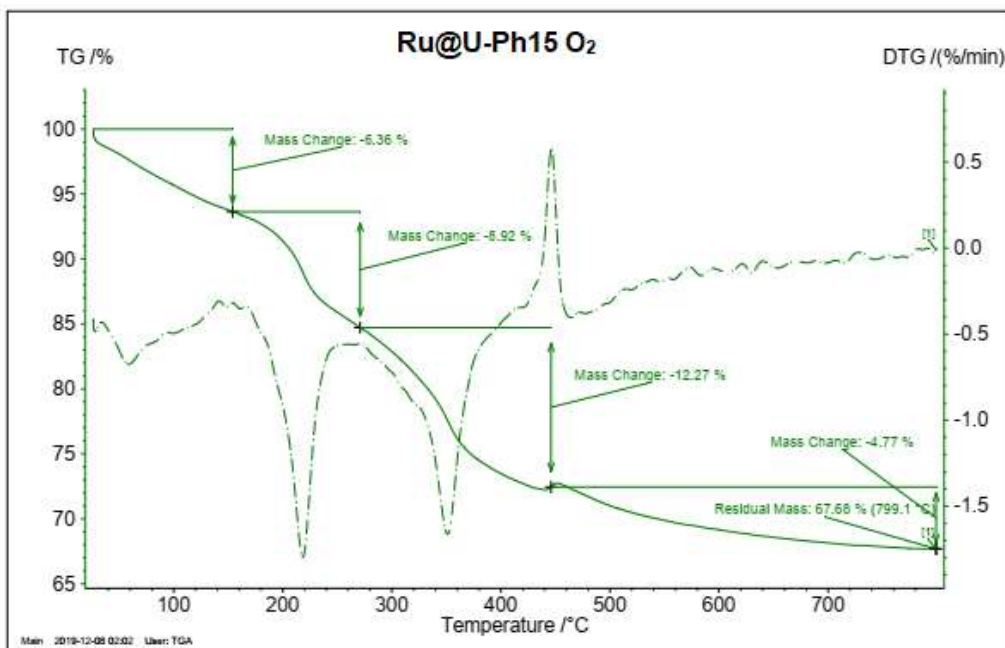


Figure S16. Thermogravimetric analysis curve of the Ru@U-Ph15 material under the oxygen atmosphere

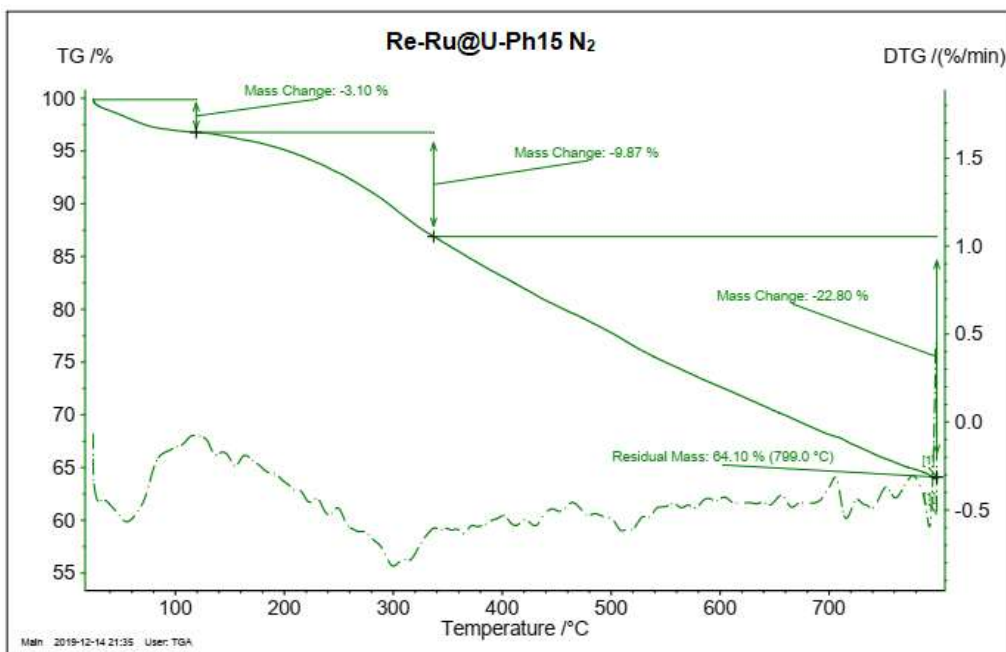


Figure S17. Thermogravimetric analysis curve of the recovered Ru@U-Ph15 material under the nitrogen atmosphere

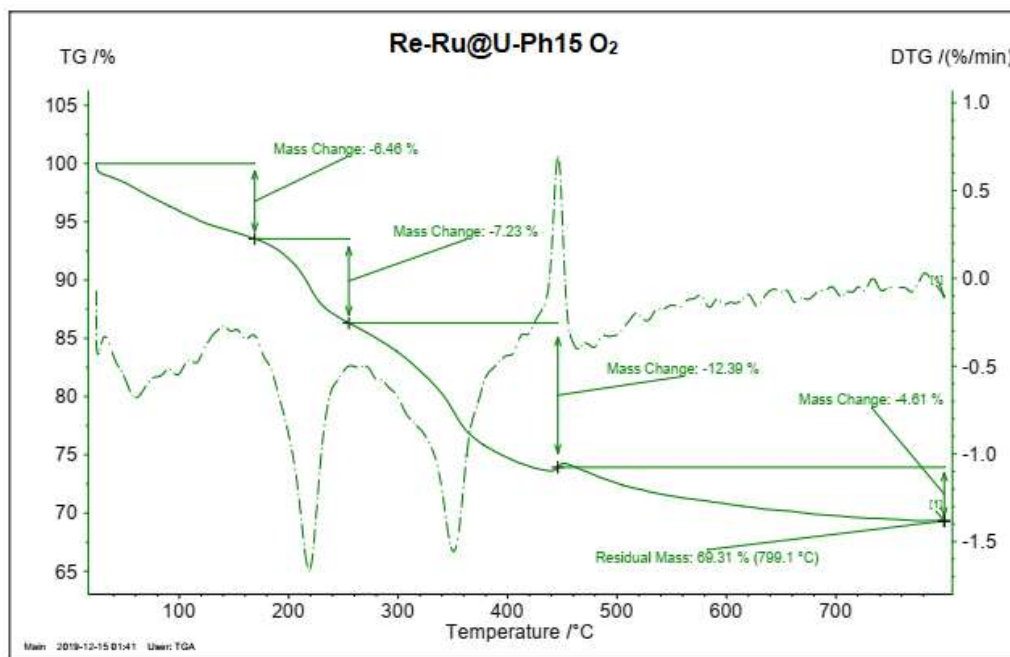


Figure S18. Thermogravimetric analysis curve of the recovered Ru@U-Ph15 material under the oxygen atmosphere

Table S1. Ru loading of Ru@BFPMOs obtained by ICP-AES

Materials	Concentration of Ru (ppm)	mmol.g ⁻¹ (Ru)
Ru@U-Et15	9.26	0.2292
Ru@P-Et15	7.01	0.1735
Ru@U-Ph15	7.77	0.1923
Ru@P-Ph15	6.96	0.1722

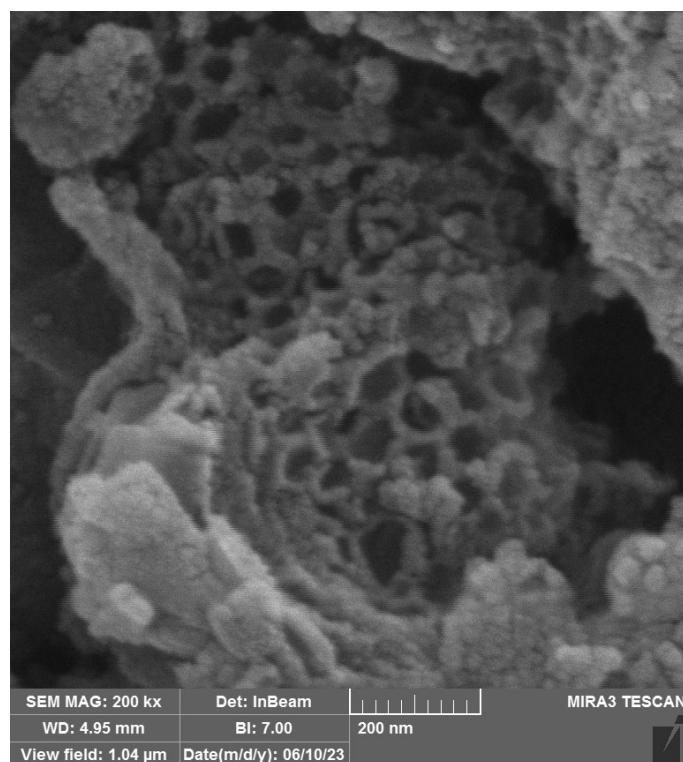


Figure S19. SEM image of the Ru@U-Ph15 (scale bar: 200 nm).

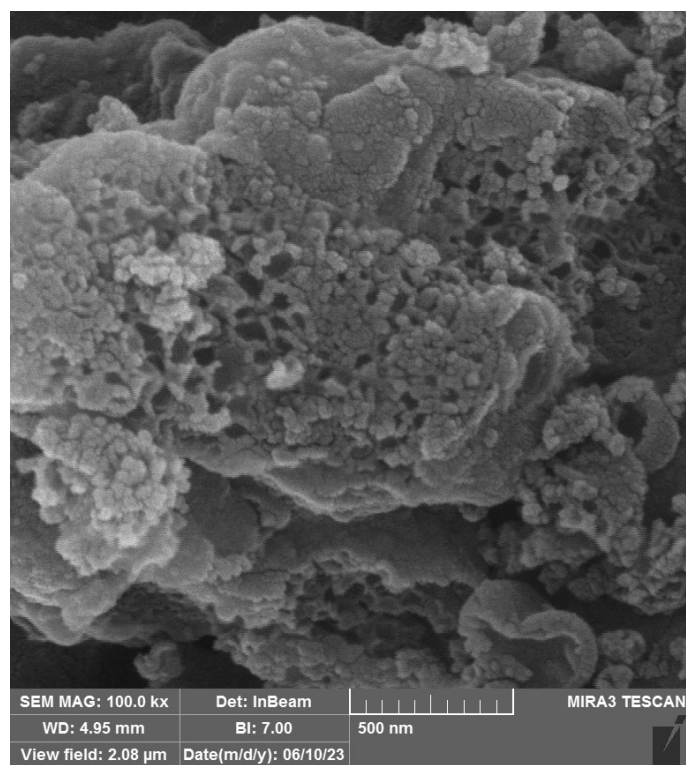


Figure S20. SEM image of the Ru@U-Ph15 (scale bar: 500 nm).

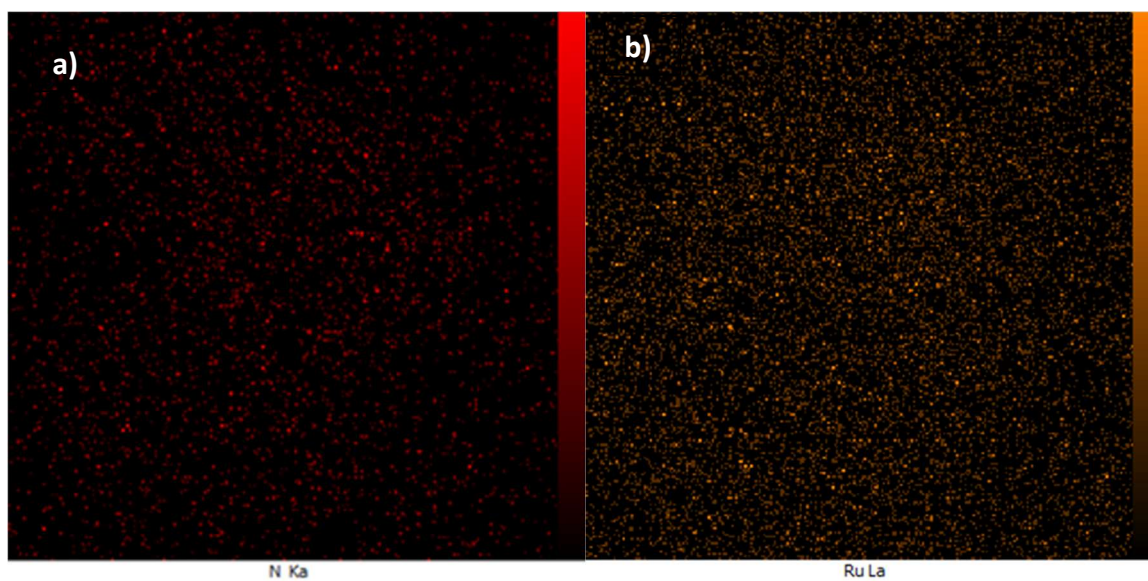


Figure S21. EDX Elemental mapping of (a) Nitrogen and (b) Ruthenium of the Ru@U-Ph15 Catalyst.

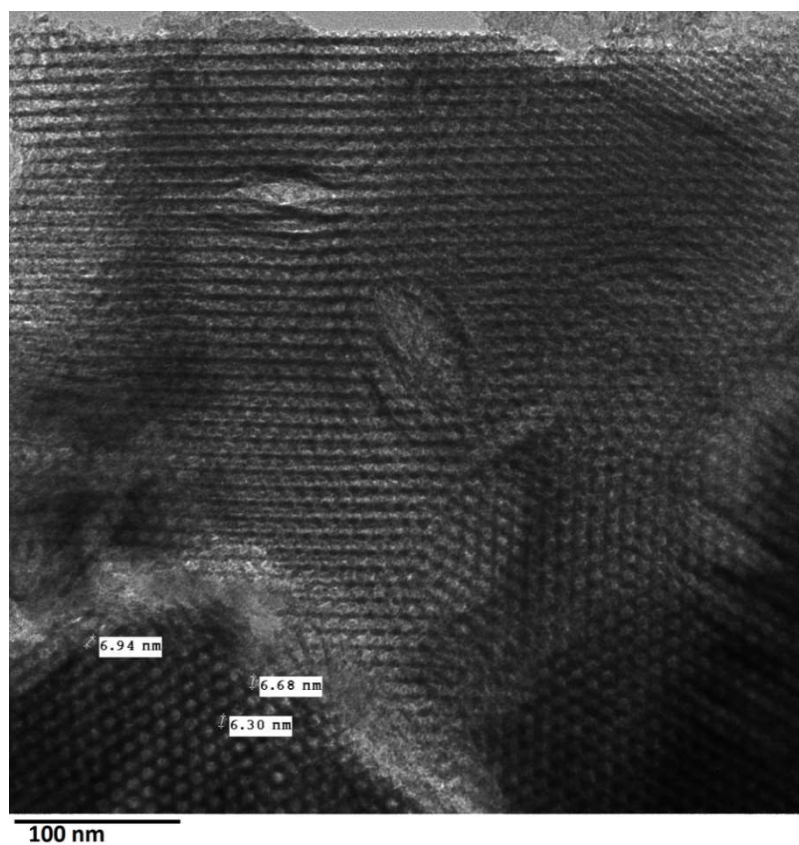


Figure S22. HRTEM image of the Unplugged Ph-BFPMO (scale bar: 100 nm).

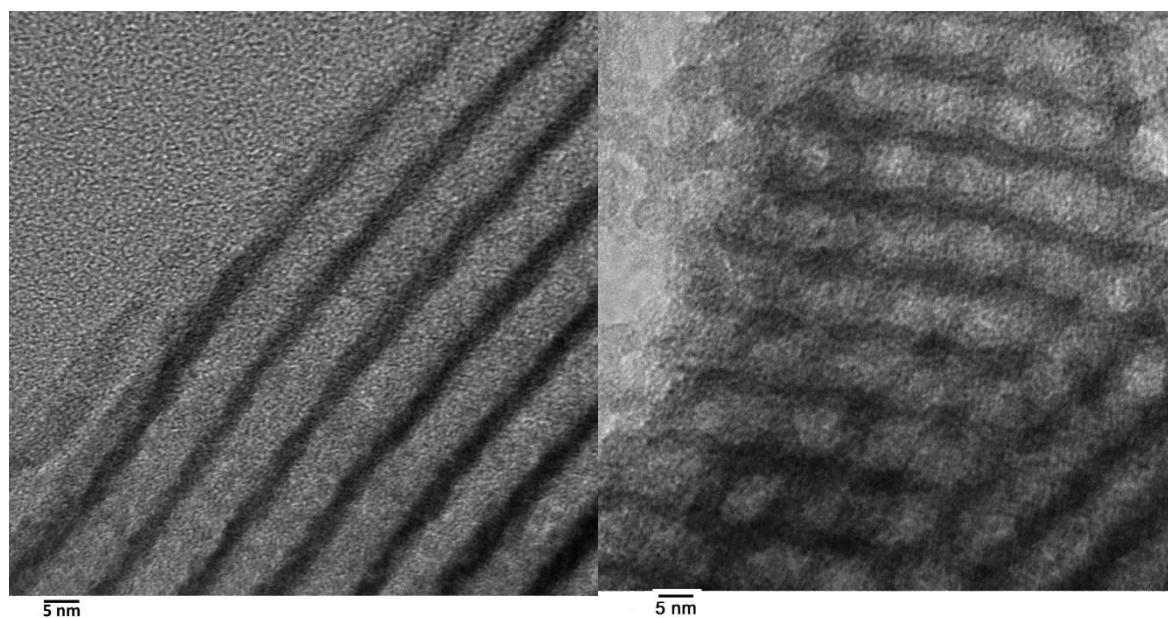


Figure S23. HRTEM image of the Unplugged Ph-BFPMO with 2D hexagonal structure and uniform cylindrical mesochannels (scale bar: 5 nm).

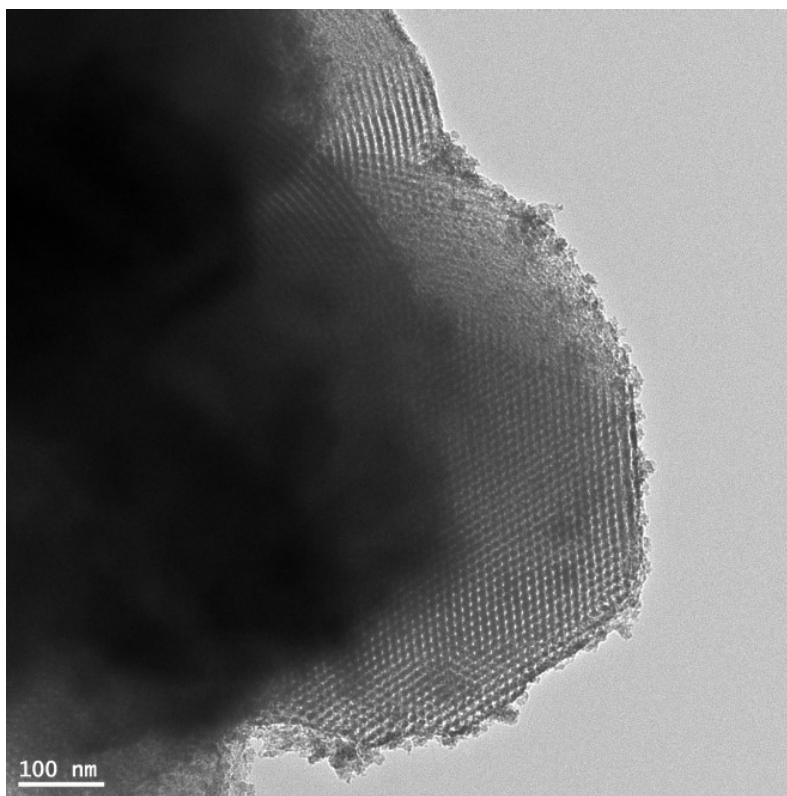


Figure S24. HRTEM image of the Ru@U-Ph15 (scale bar: 100 nm).

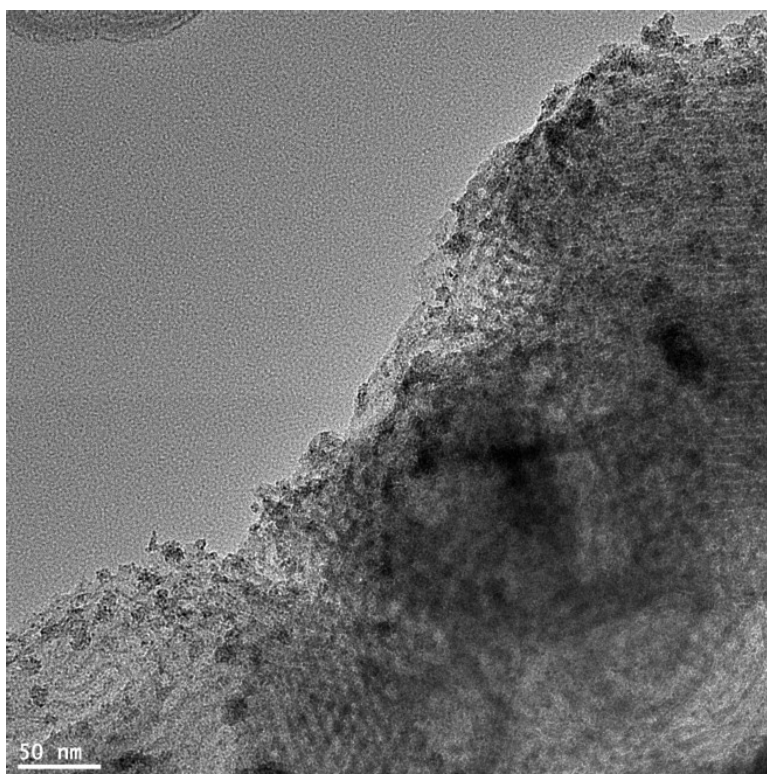


Figure S25. HRTEM image of the Ru@U-Ph15 (scale bar: 50 nm).

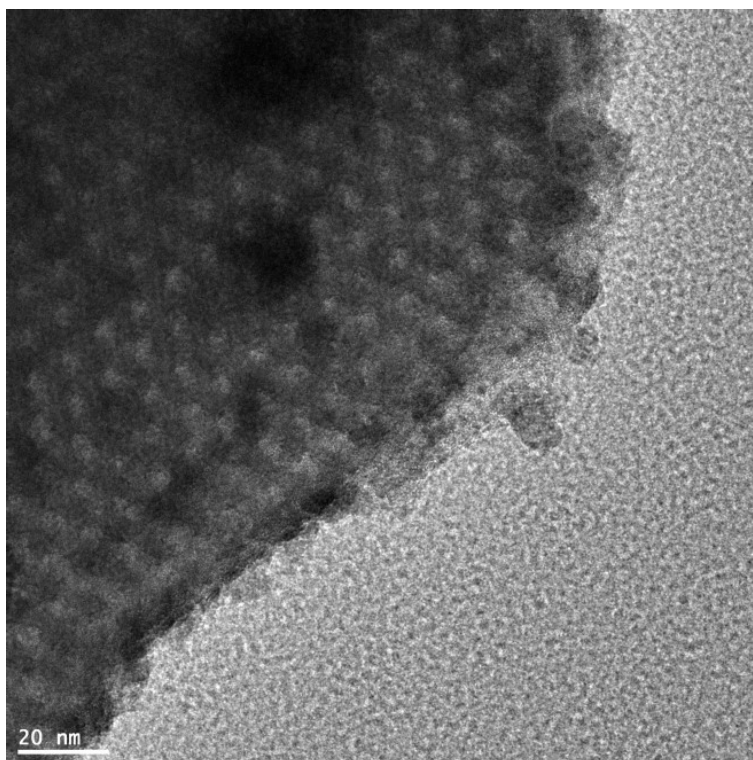


Figure S26. HRTEM image of the Ru@U-Ph15 (scale bar: 20 nm).

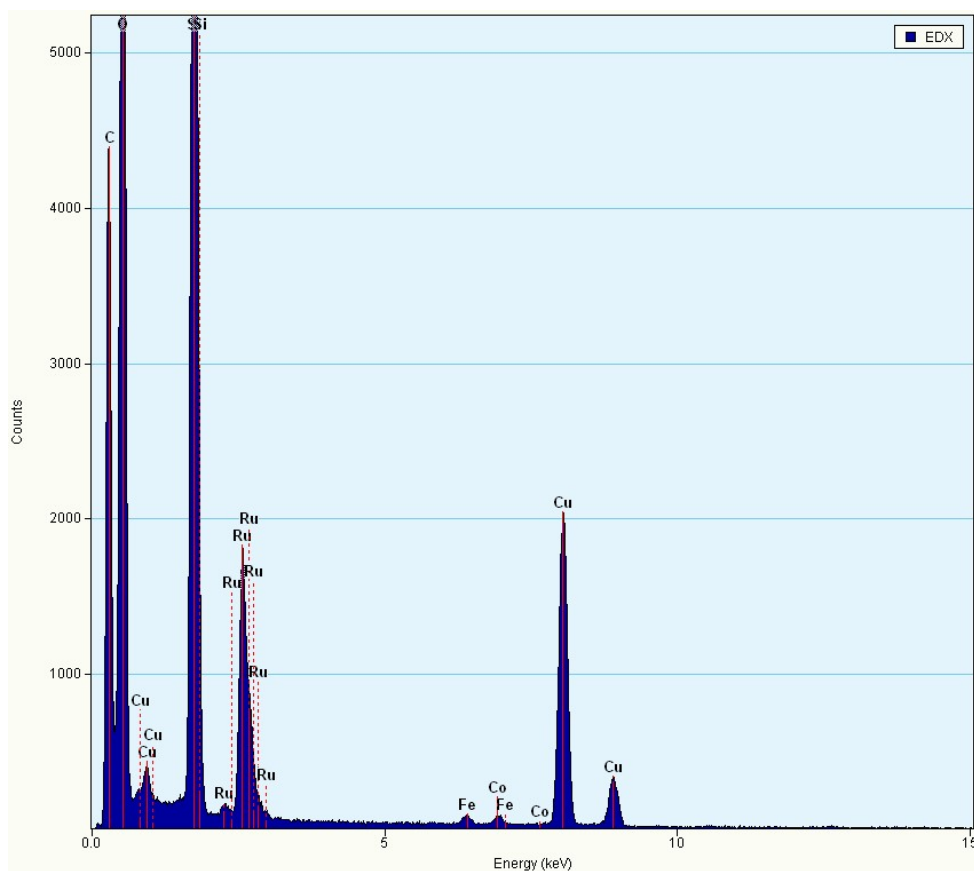


Figure S27. Energy-dispersive X-ray spectroscopy (EDS) of Ru@U-Ph15

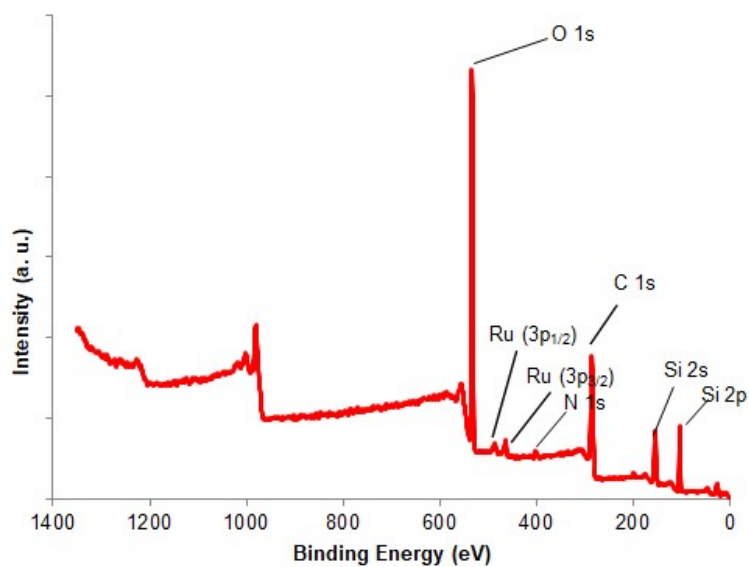


Figure S28. XPS survey spectrum of Ru@U-Ph15

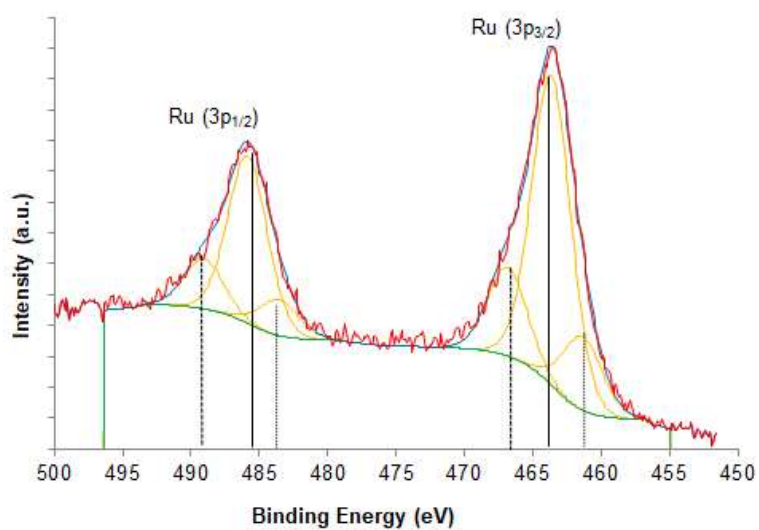


Figure S29. High-resolution XPS spectrum of Ru3p of Ru@U-Ph15

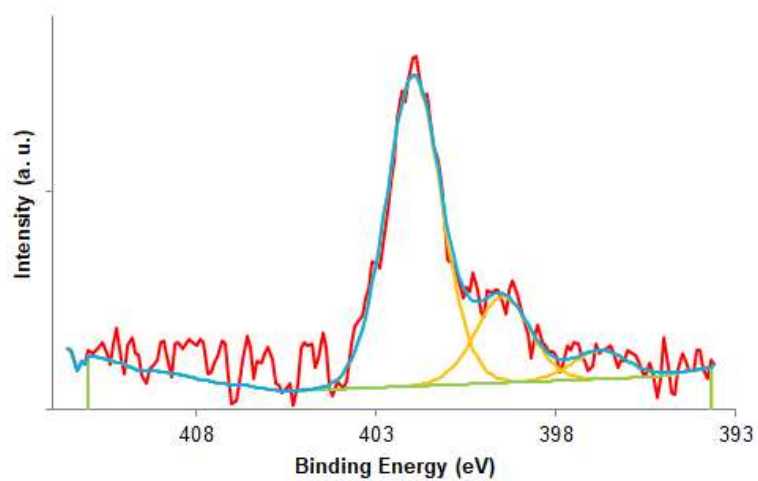


Figure S30. High-resolution XPS spectrum of N1s of Ru@U-Ph15

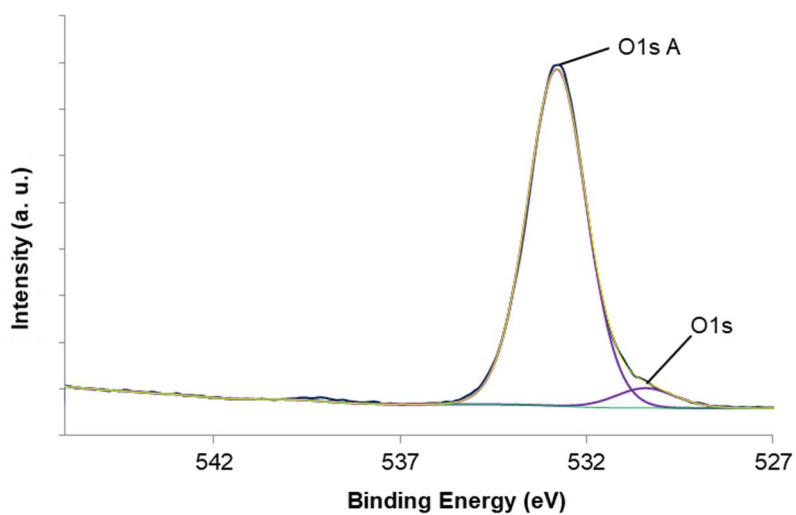


Figure S31. High-resolution XPS spectrum of O1s of Ru@U-Ph15

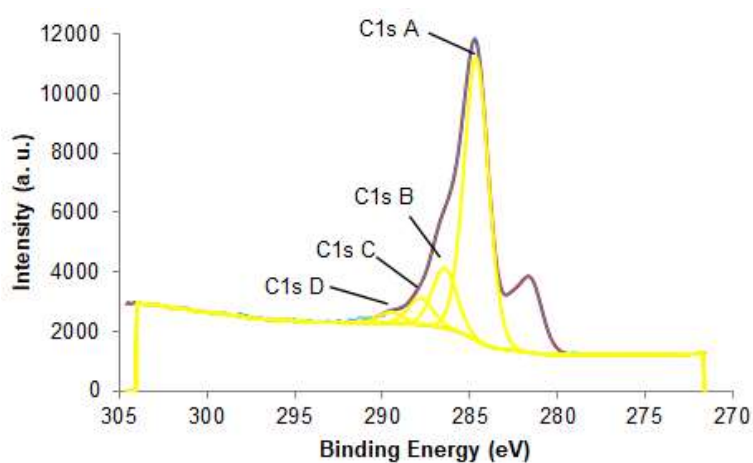


Figure S32. High-resolution XPS spectrum of C1s of Ru@U-Ph15

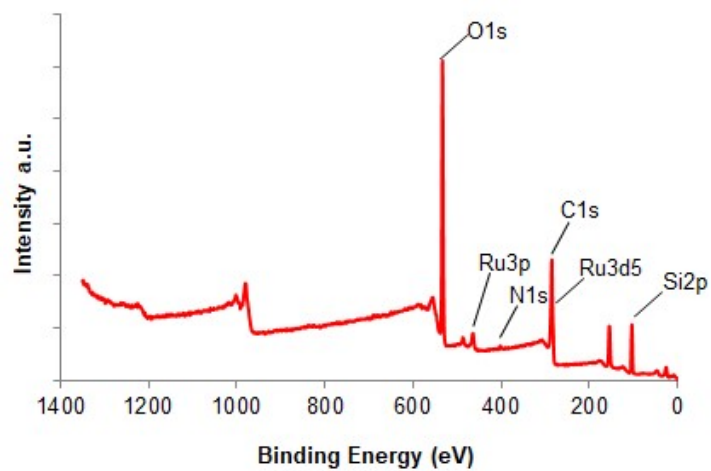


Figure S33. XPS survey spectrum of Re-Ru@U-Ph15

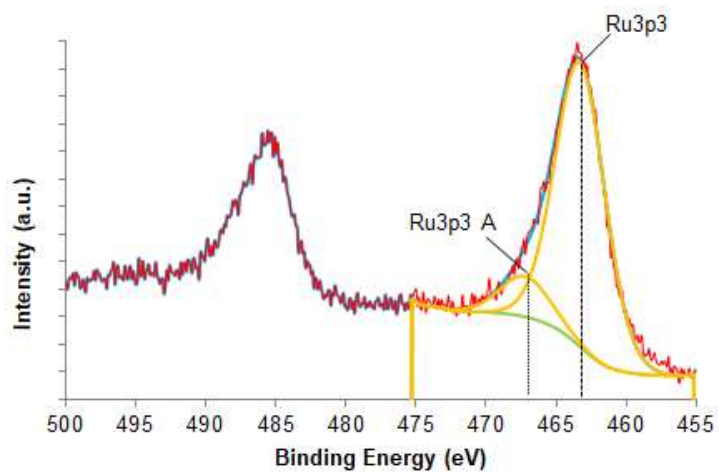


Figure S34. High-resolution XPS spectrum of Ru3p of Re-Ru@U-Ph15

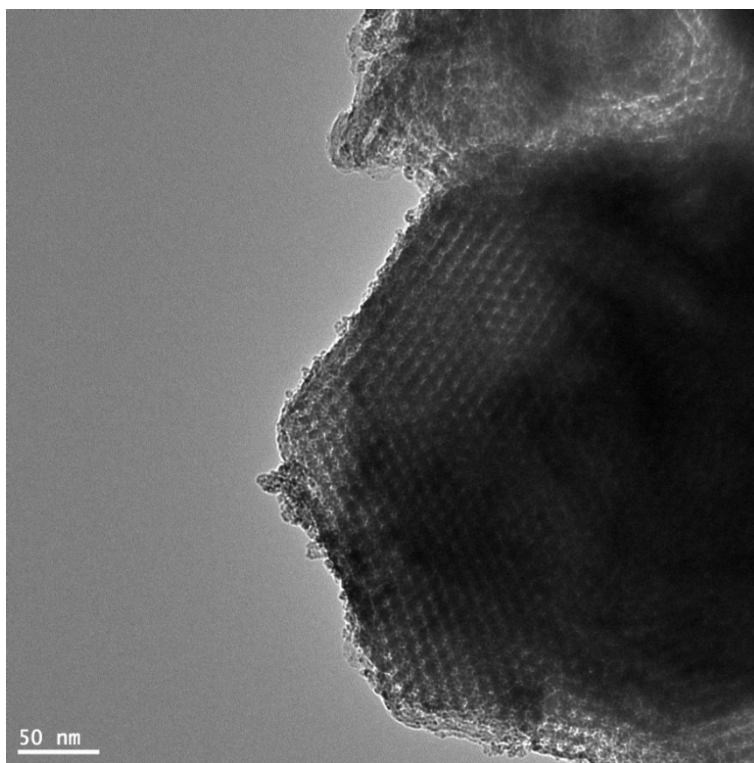


Figure S35. HRTEM image of the Re-Ru@U-Ph15 (scale bar: 50 nm).

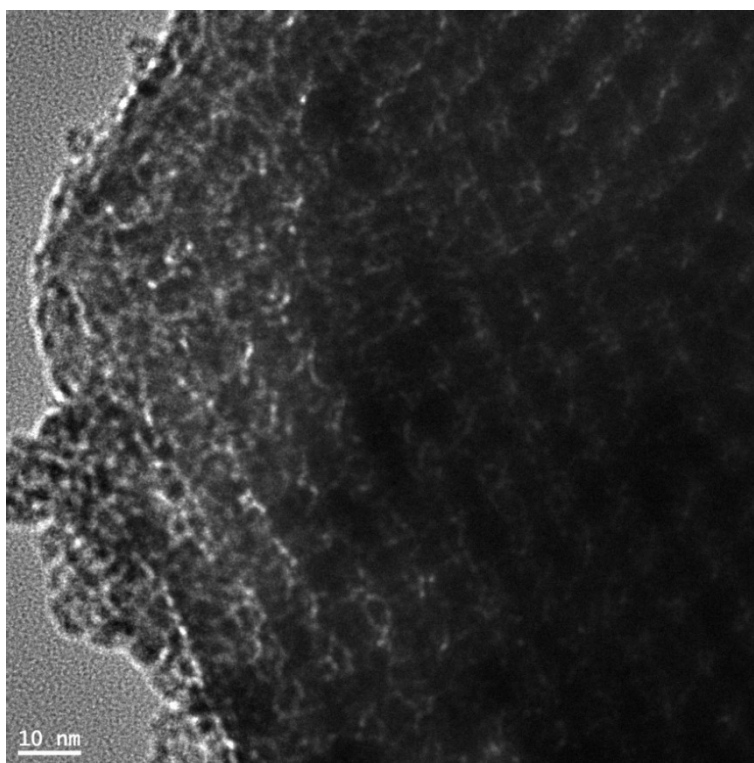


Figure S36. HRTEM image of the Re-Ru@U-Ph15 (scale bar: 10 nm).

Table S2. Comparison of several Ru-based catalytic systems in the oxidation of alcohols into the corresponding carbonyl compounds

Entry	Catalyst (mg, mol %)	Reaction conditions	Type of alcohols	Reusability	Ref.
1	Ru/Al ₂ O ₃ (2.5 mol%)	Trifluorotoluene, O ₂ (1 atm), 83 °C	18 substrates (including primary and secondary benzylic and aliphatic alcohols, allylic and heterocyclic alcohols)	7 cycles without drop in reaction yield and selectivity	[3]
2	rGO@Ru-RMβ-CD (80 mg, 2 mol% Ru)	K ₂ CO ₃ , water, O ₂ balloon, 85 °C	22 substrates (including primary and secondary benzylic alcohols, and propargylic alcohols)	5 cycle with a drop in reaction yield after the third cycle	[4]
3	Ru@PMO-IL (80 mg, 2.5 mol %)	Trifluorotoluen, O ₂ , 70 °C	24 substrates (including primary and secondary benzylic and aliphatic alcohols, allylic and heterocyclic alcohols)	5 cycle with a drop in reaction yield after the third cycle	[2]
4	ZC-Ru ^a (300 mg, (2.4 wt % Ru)	Toluene, O ₂ (1 atm), 80 °C	10 substrates (including primary and secondary benzylic and aliphatic alcohols, allylic and heterocyclic alcohols)	5 cycles without drop in reaction yield and selectivity	[5]
5	Ru@ Anodic Aluminum Oxide (20 mg, 2.3 wt % Ru)	Toluene, air flow (1 atm), 50 °C	18 substrates (including primary and secondary benzylic alcohols, secondary aliphatic alcohols, allylic and heterocyclic alcohols)	5 cycles without drop in reaction yield and selectivity	[6]
6	Ru@U-Ph15 (19.5 mg, 1.5 mol %)	Toluene, O₂, 90 °C	32 substrates (including primary and secondary benzylic and aliphatic alcohols, allylic and heterocyclic alcohols)	5 cycles with a steadily drop in reaction yield	This work

^aZeolite confined nanostructured dinuclear ruthenium clusters

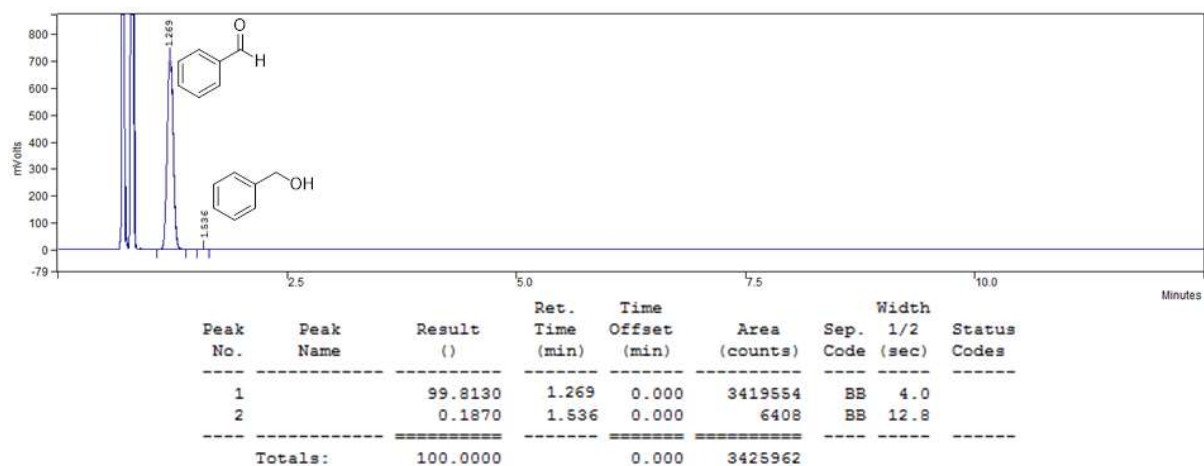


Figure S37. Gas chromatogram of benzyl alcohol reaction (Table 4, Entry 1)

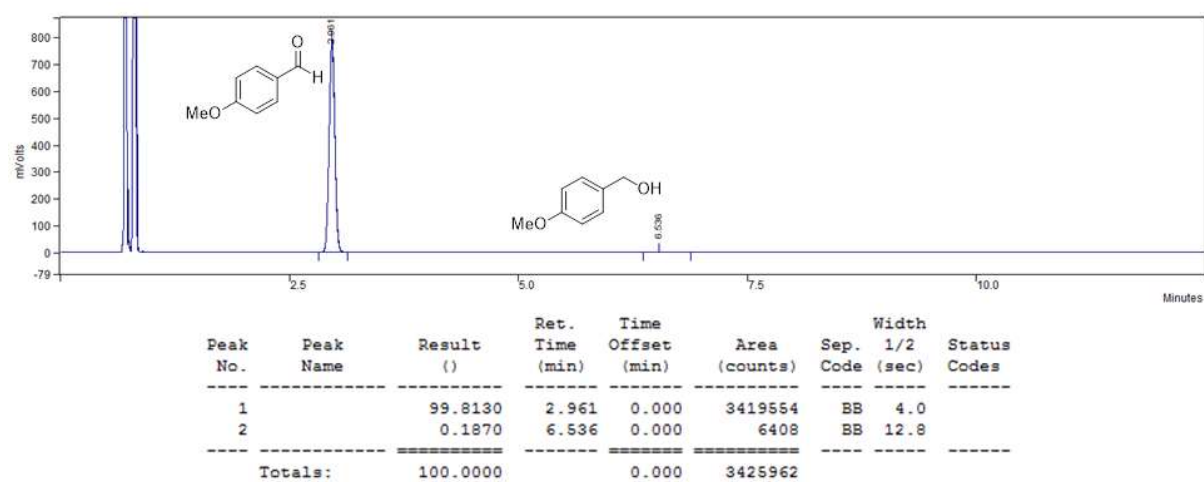


Figure S38. Gas chromatogram of 4-methoxybenzyl alcohol reaction (Table 4, Entry 2)

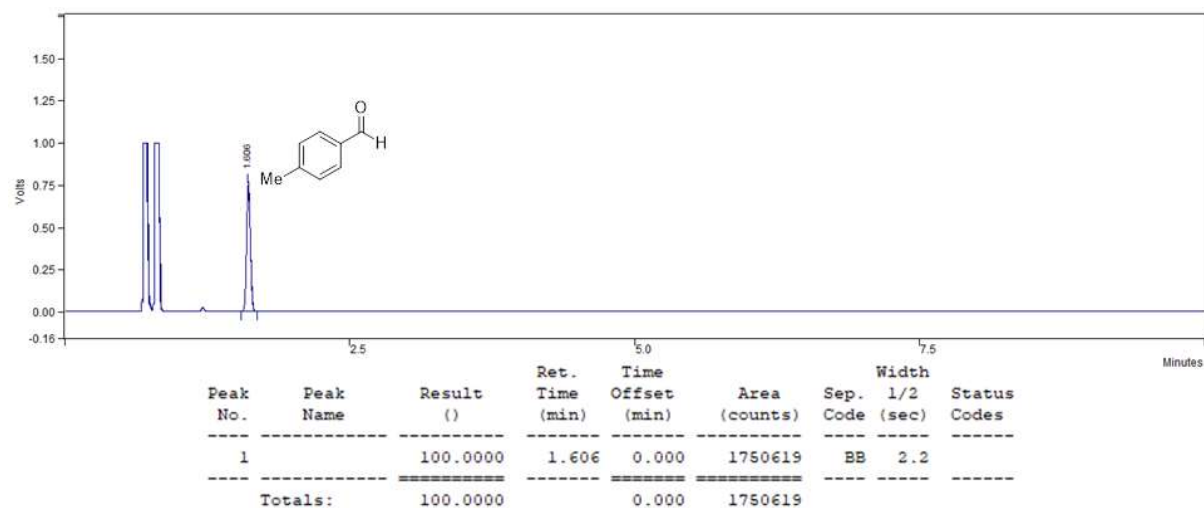


Figure S39. Gas chromatogram of 4-methylbenzyl alcohol reaction (Table 4, Entry 3)

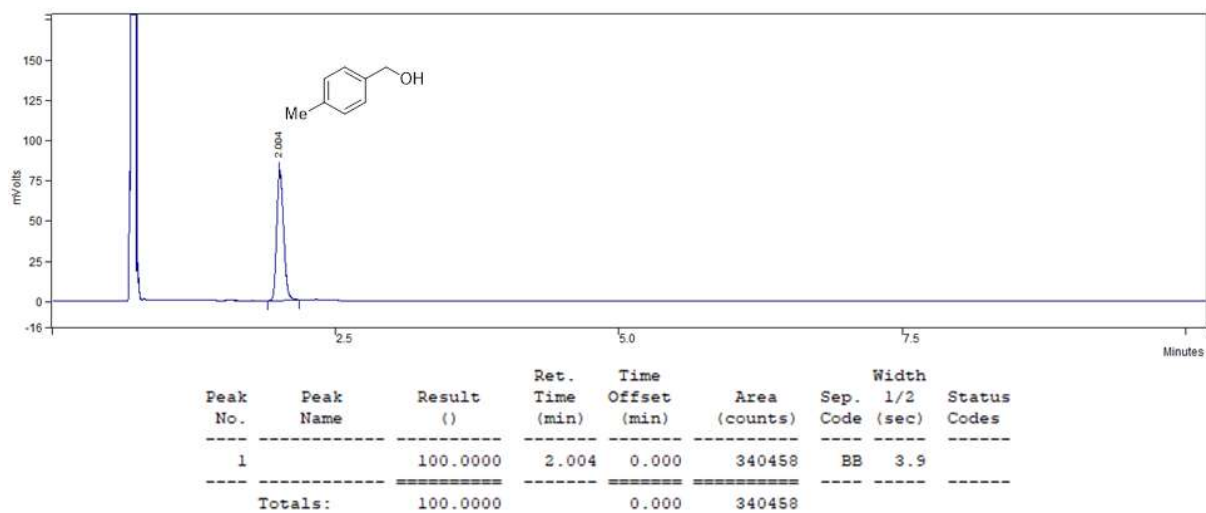


Figure S40. Gas chromatogram of 4-methylbenzyl alcohol (blank)

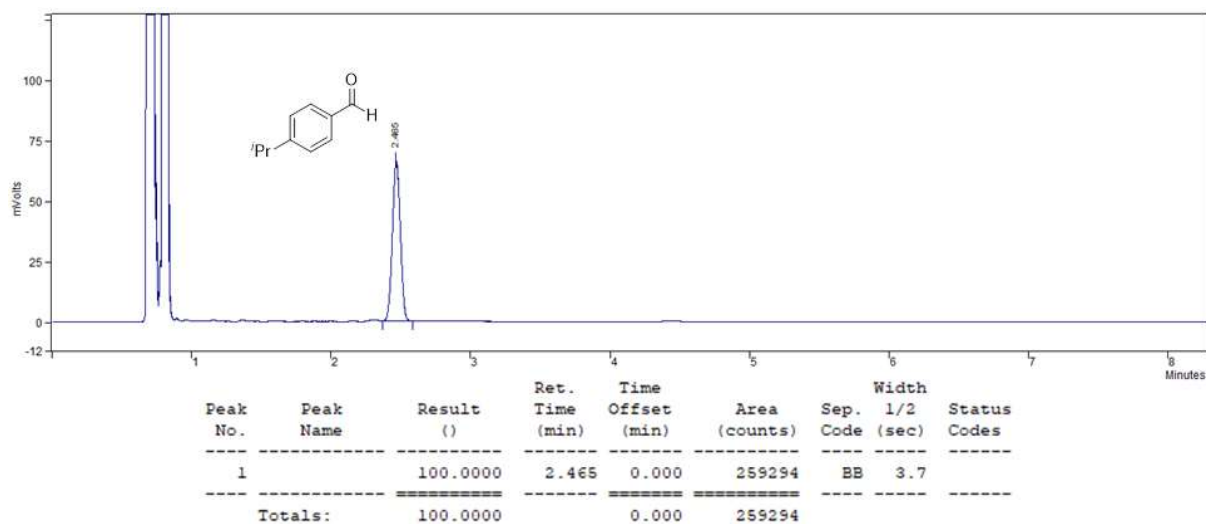


Figure S41. Gas chromatogram of 4-isopropylbenzyl alcohol reaction (Table 4, Entry 4)

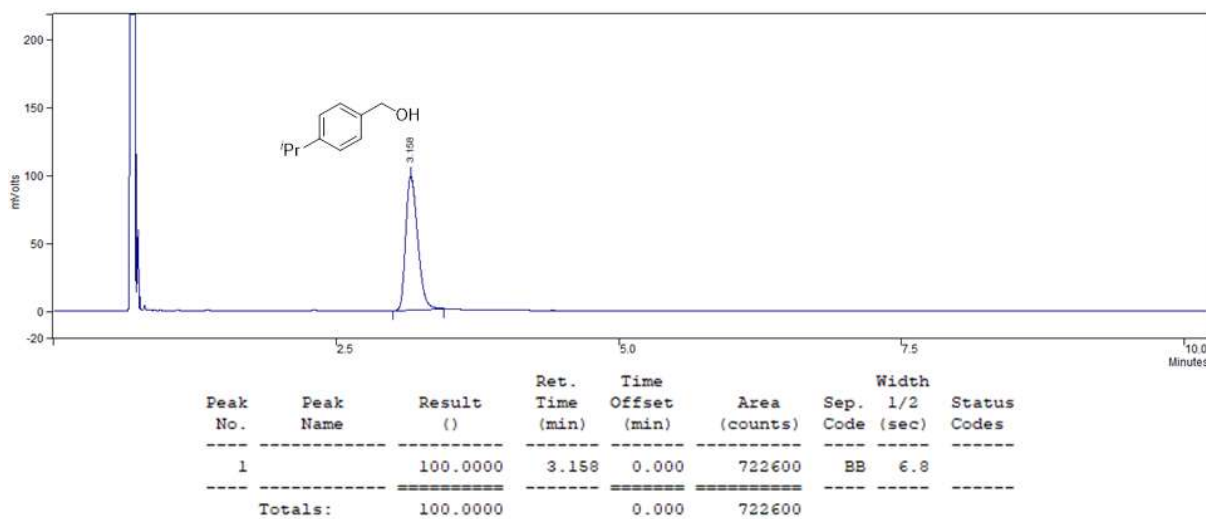


Figure S42. Gas chromatogram of 4-isopropylbenzyl alcohol (blank)

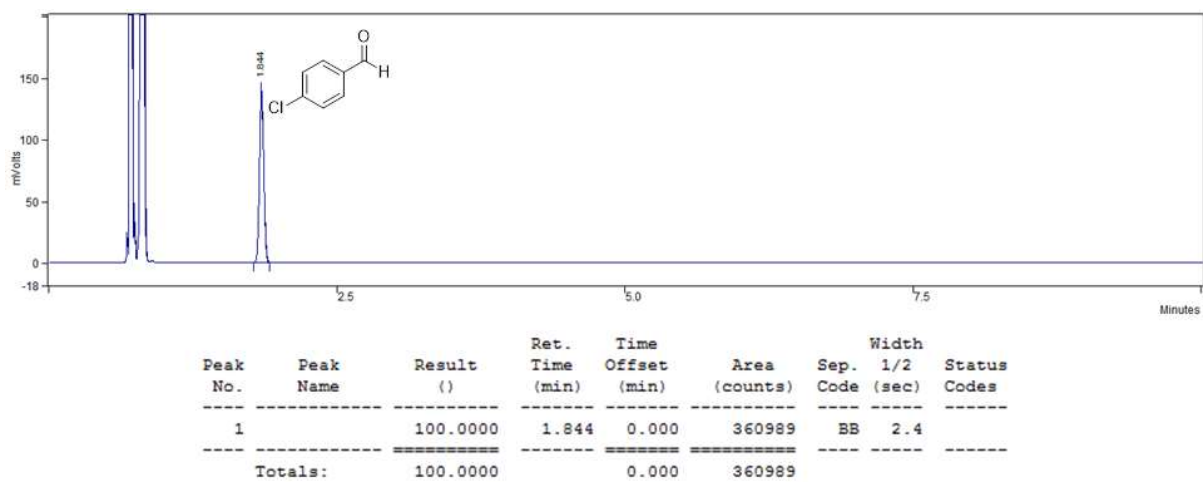


Figure S43. Gas chromatogram of 4-chlorobenzyl alcohol reaction (Table 4, Entry 5)

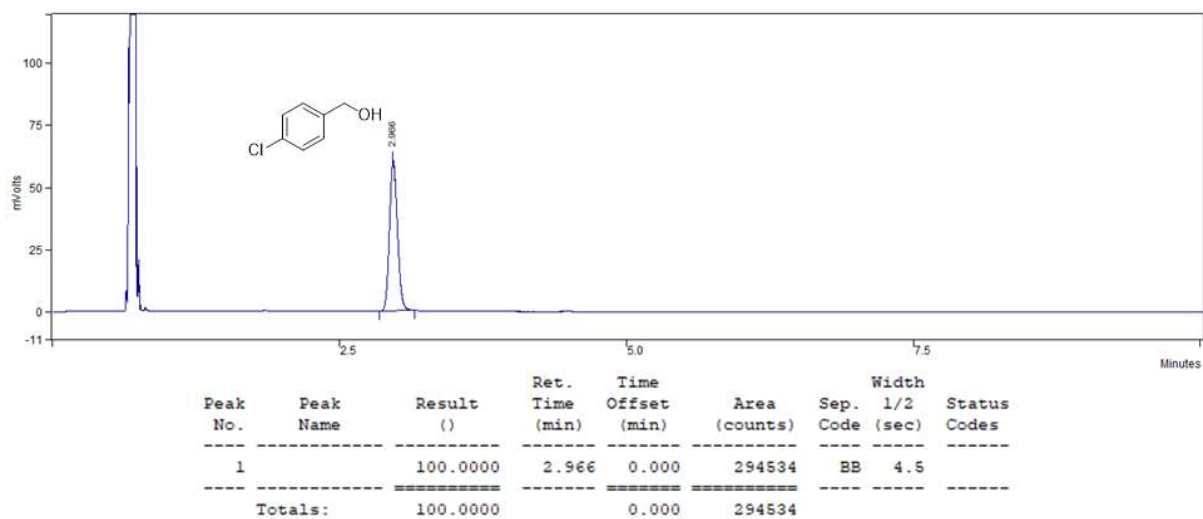


Figure S44. Gas chromatogram of 4-chlorobenzyl alcohol (blank)

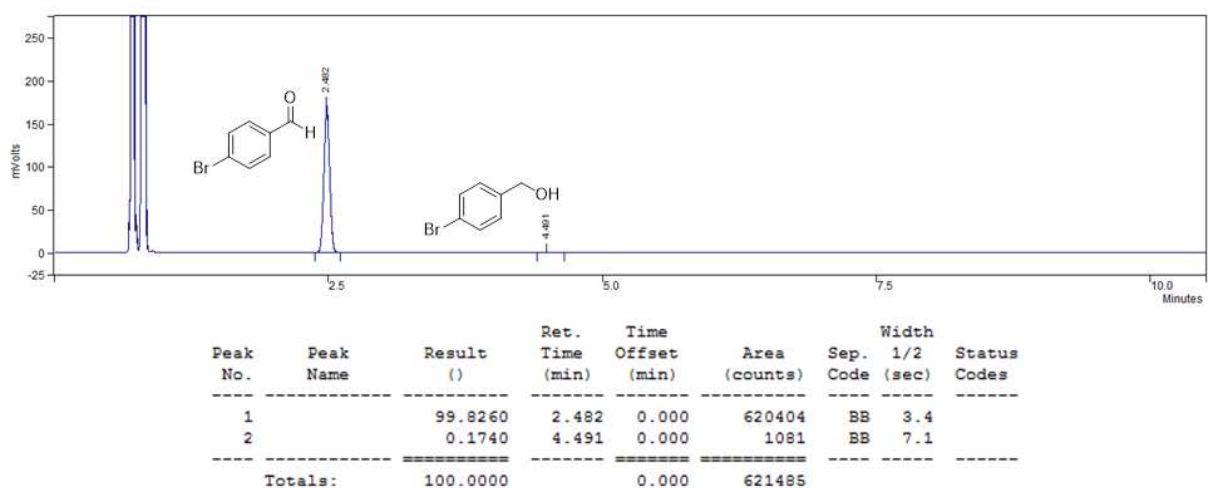


Figure S45. Gas chromatogram of 4-bromobenzyl alcohol reaction (Table 4, Entry 6)

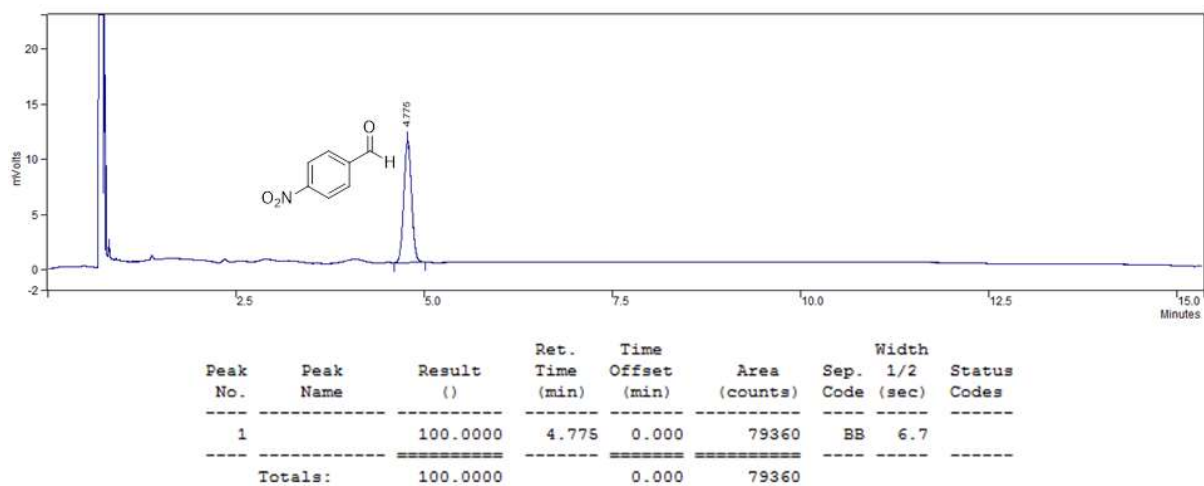


Figure S46. Gas chromatogram of 4-nitrobenzyl alcohol reaction (Table 4, Entry 7)

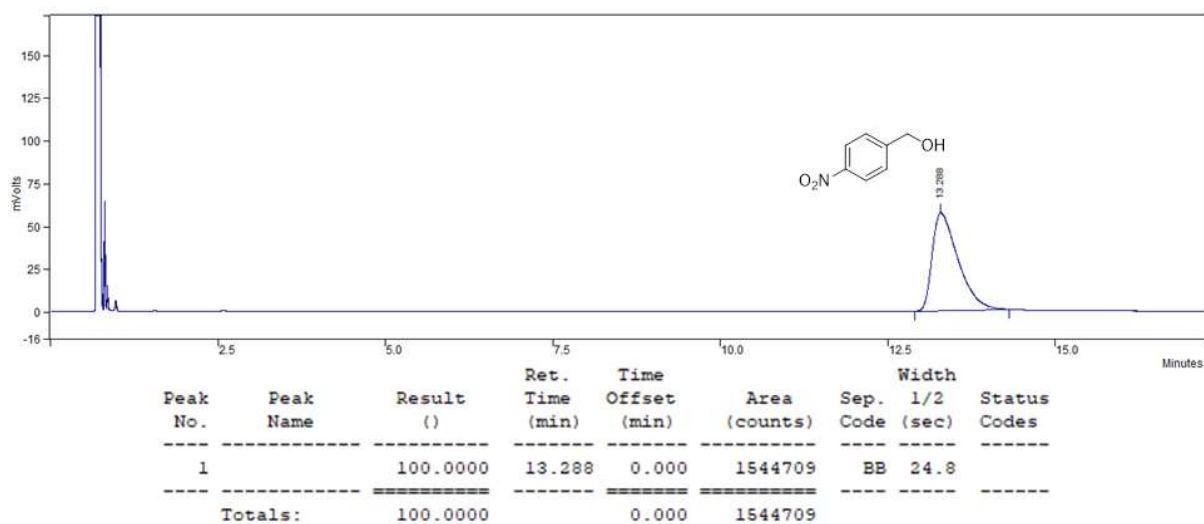


Figure S47. Gas chromatogram of 4-nitrobenzyl alcohol (blank)

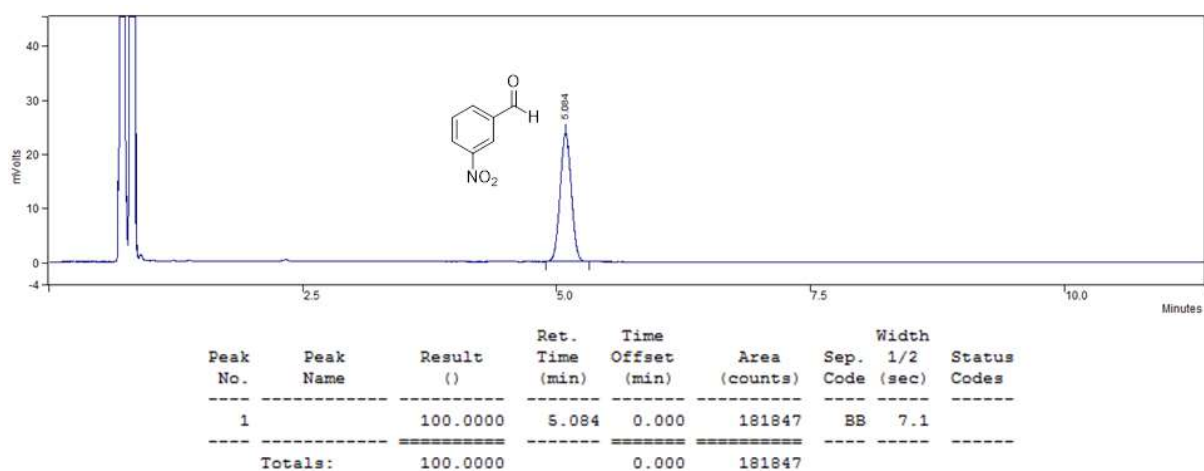


Figure S48. Gas chromatogram of 3-nitrobenzyl alcohol reaction (Table 4, Entry 8)

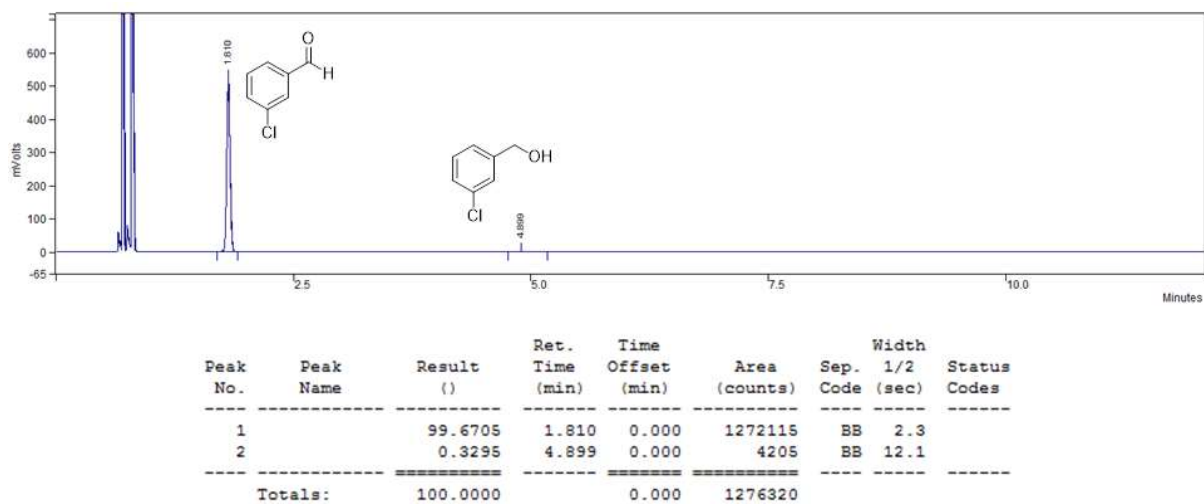


Figure S49. Gas chromatogram of 3-chlorobenzyl alcohol reaction (Table 4, Entry 9)

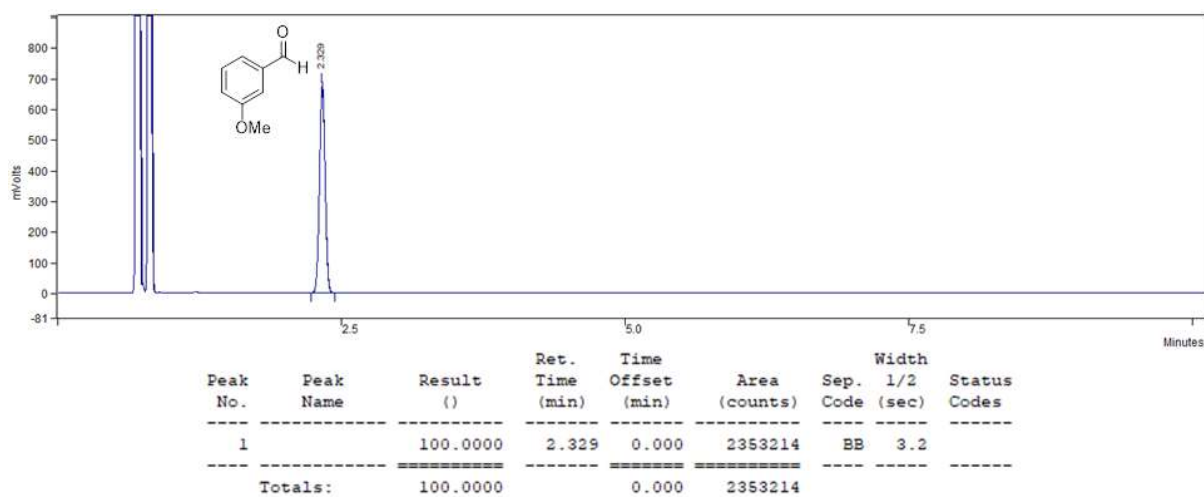


Figure S50. Gas chromatogram of 3-methoxybenzyl alcohol reaction (Table 4, Entry 10)

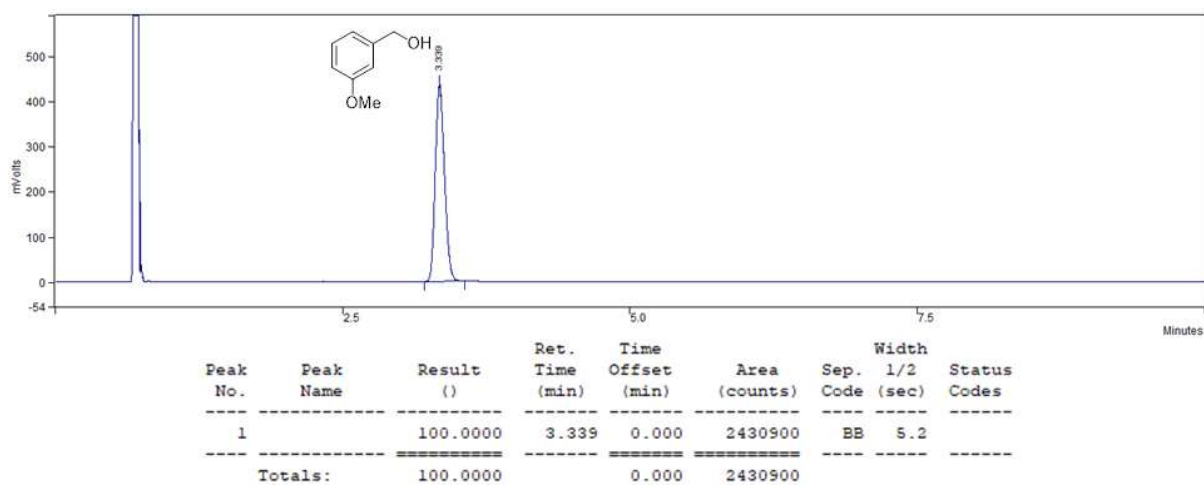


Figure S51. Gas chromatogram of 3-methoxybenzyl alcohol (blank)

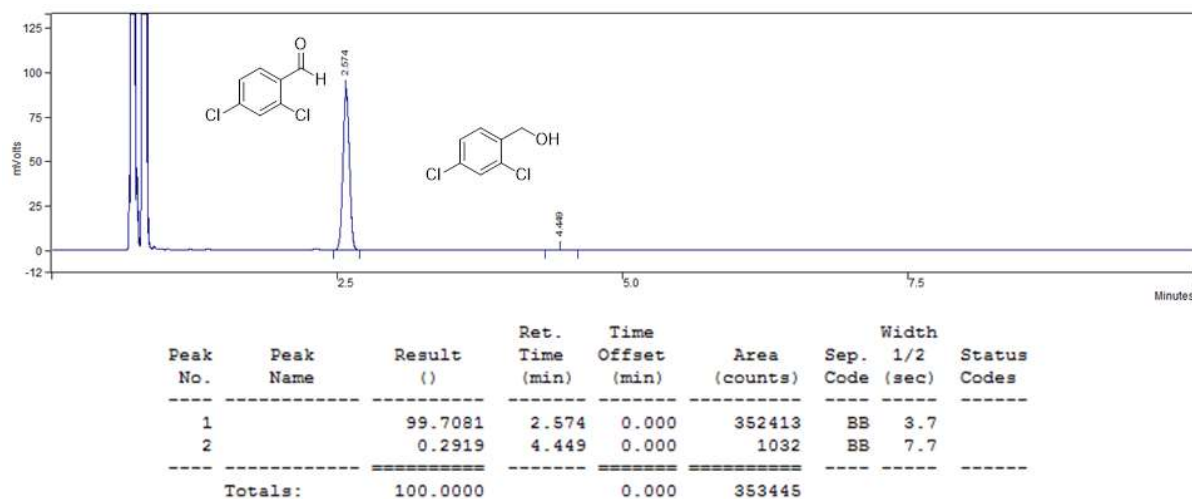


Figure S52. Gas chromatogram of 2,4-dichlorobenzyl alcohol reaction (Table 4, Entry 11)

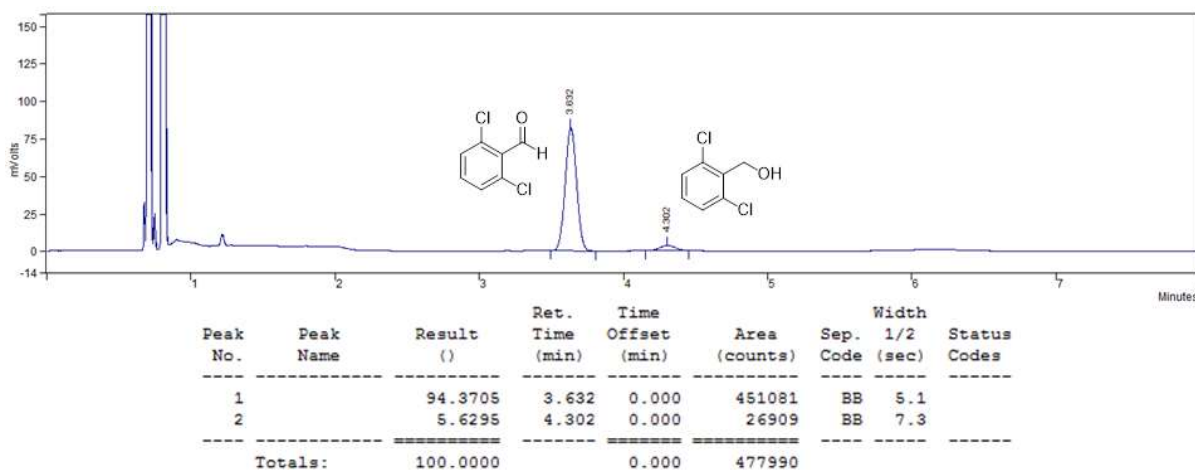


Figure S53. Gas chromatogram of 2,6-dichlorobenzyl alcohol reaction (Table 4, Entry 12)

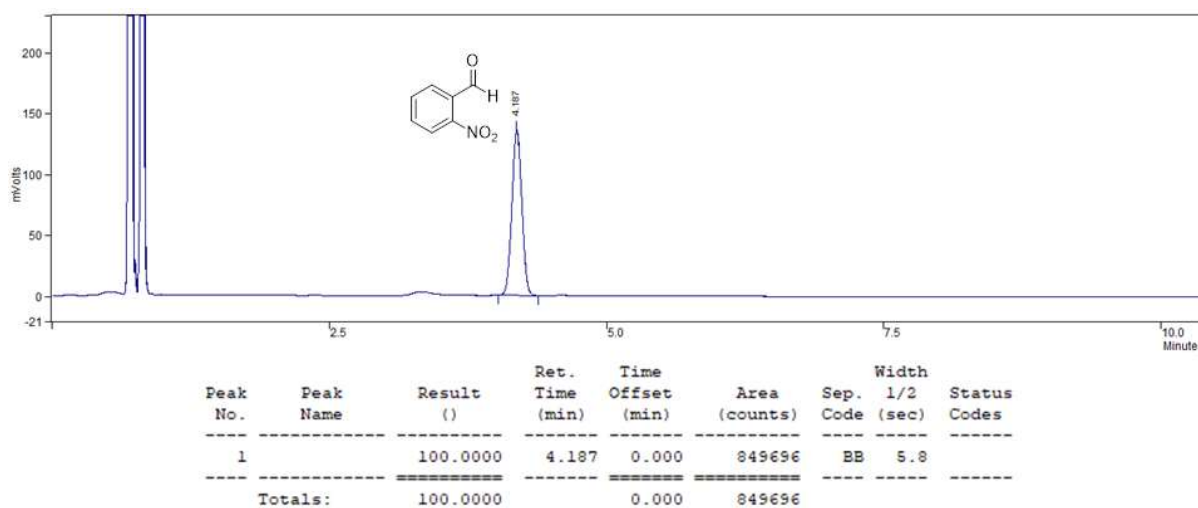


Figure S54. Gas chromatogram of 2-nitrobenzyl alcohol reaction (Table 4, Entry 13)

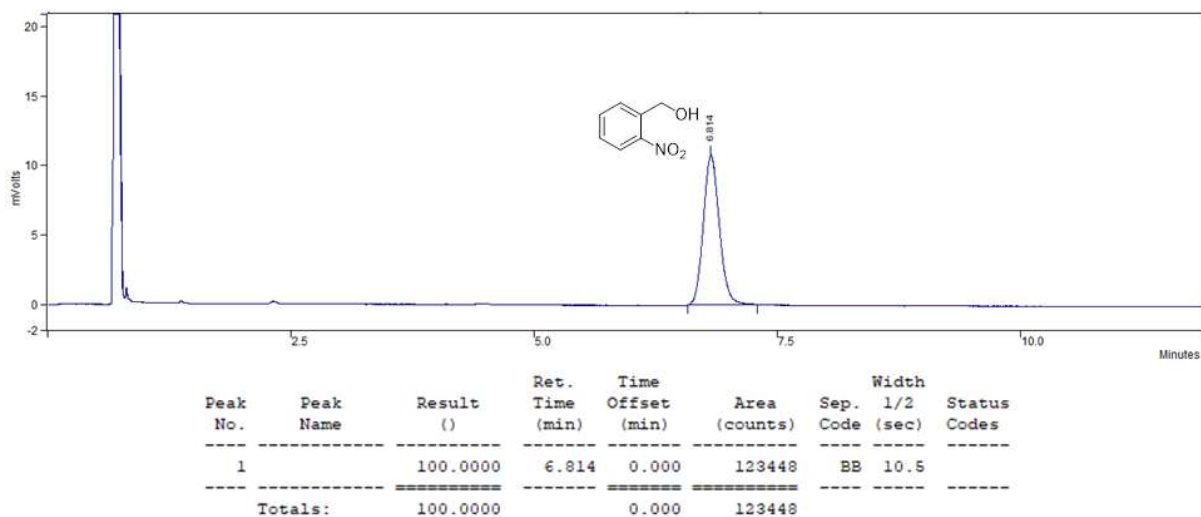


Figure S55. Gas chromatogram of 2-nitrobenzyl alcohol (blank)

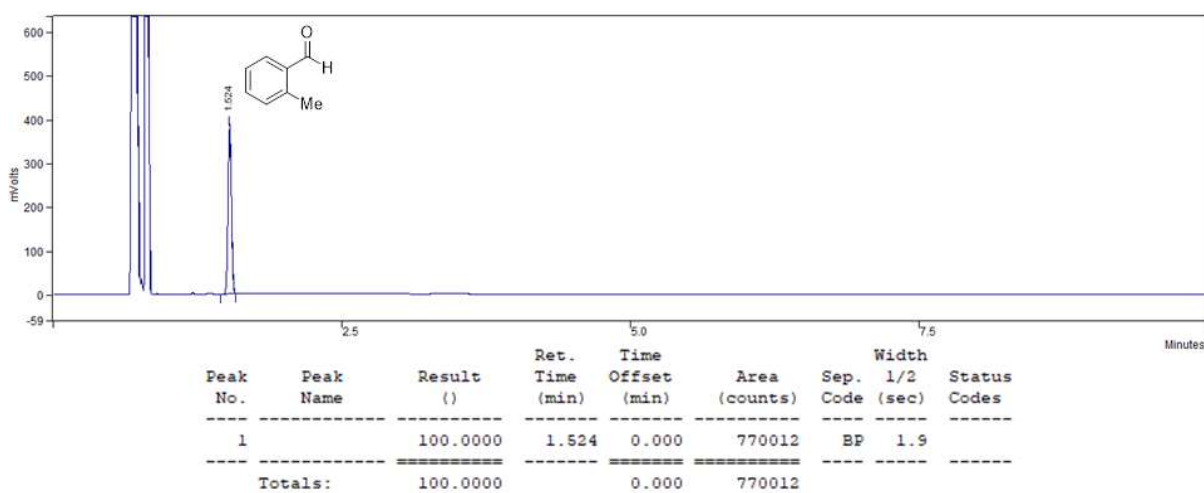


Figure S56. Gas chromatogram of 2-methylbenzyl alcohol reaction (Table 4, Entry 14)

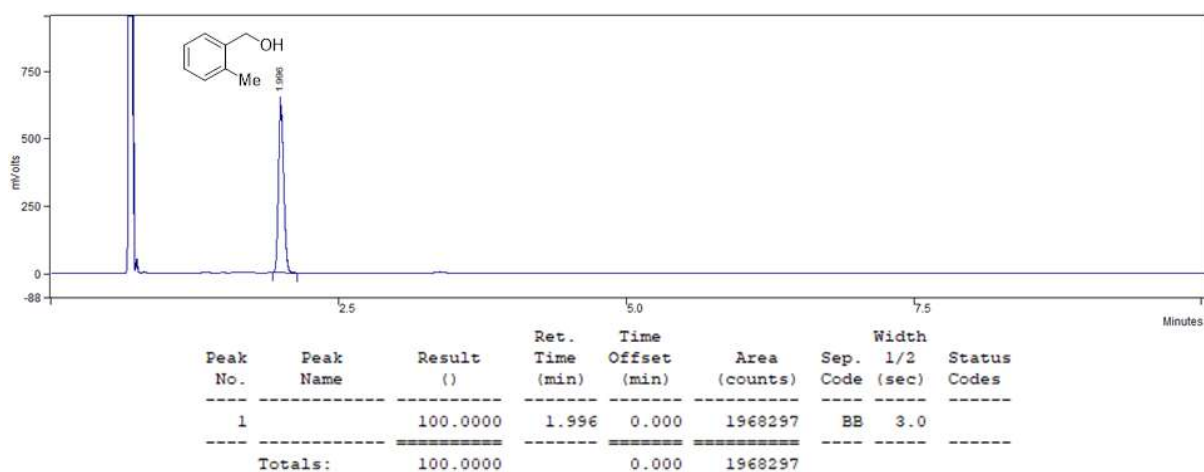


Figure S57. Gas chromatogram of 2-methylbenzyl alcohol (blank)

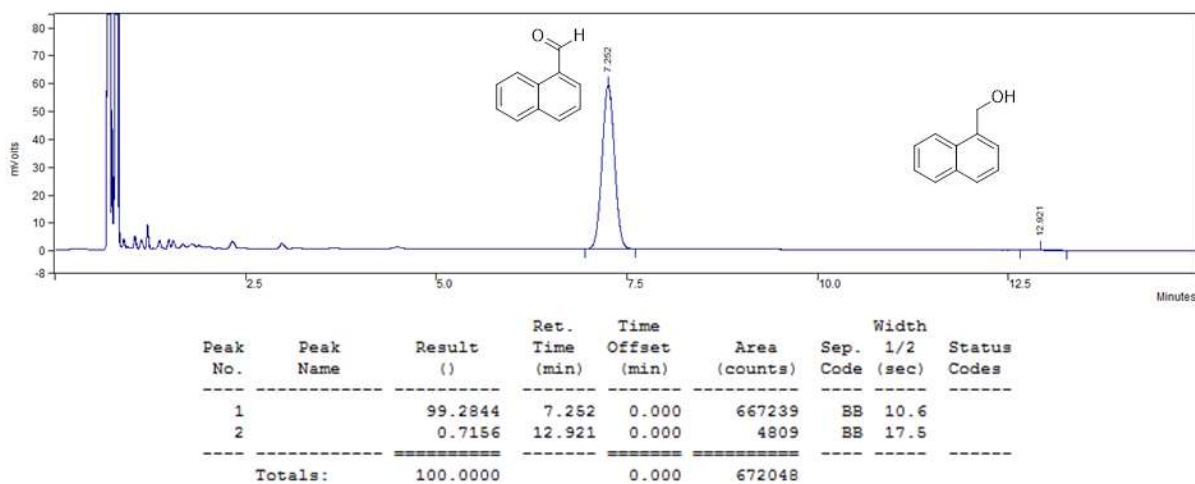


Figure S58. Gas chromatogram of 1-naphthyl methanol reaction (Table 4, Entry 15)

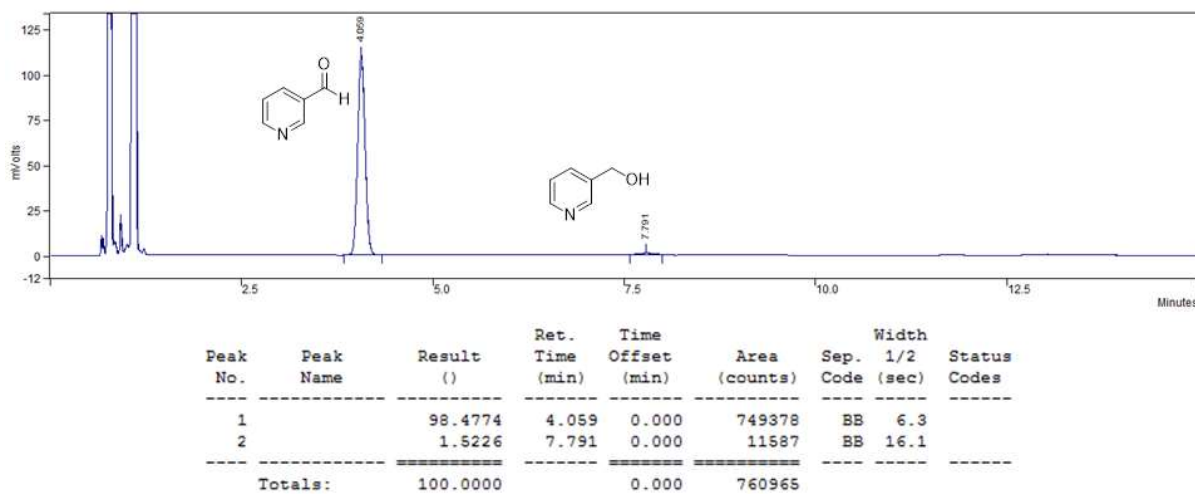


Figure S59. Gas chromatogram of 3-pyridine methanol reaction (Table 4, Entry 16)

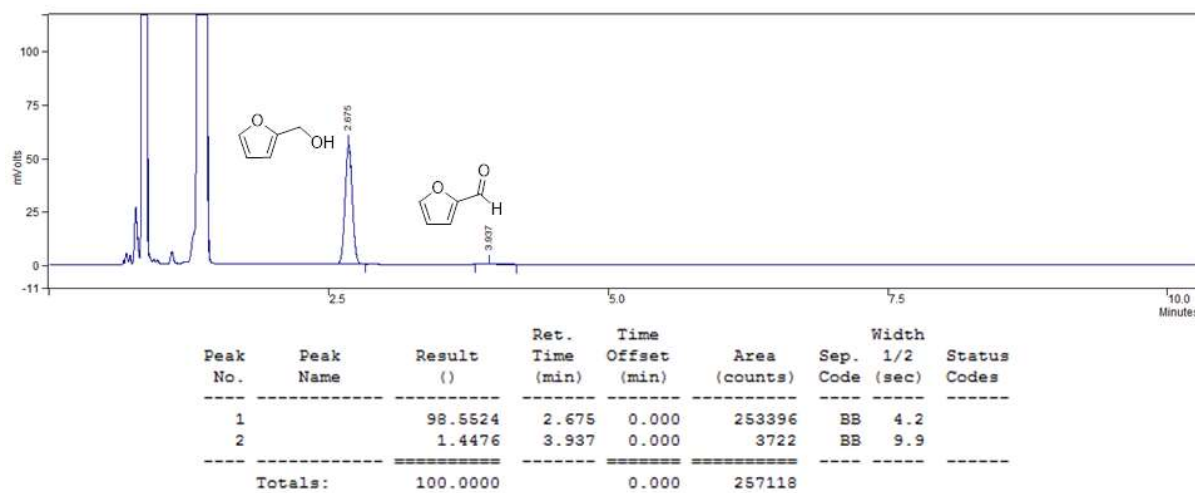


Figure S60. Gas chromatogram of 2-furyl alcohol reaction (Table 4, Entry 17)

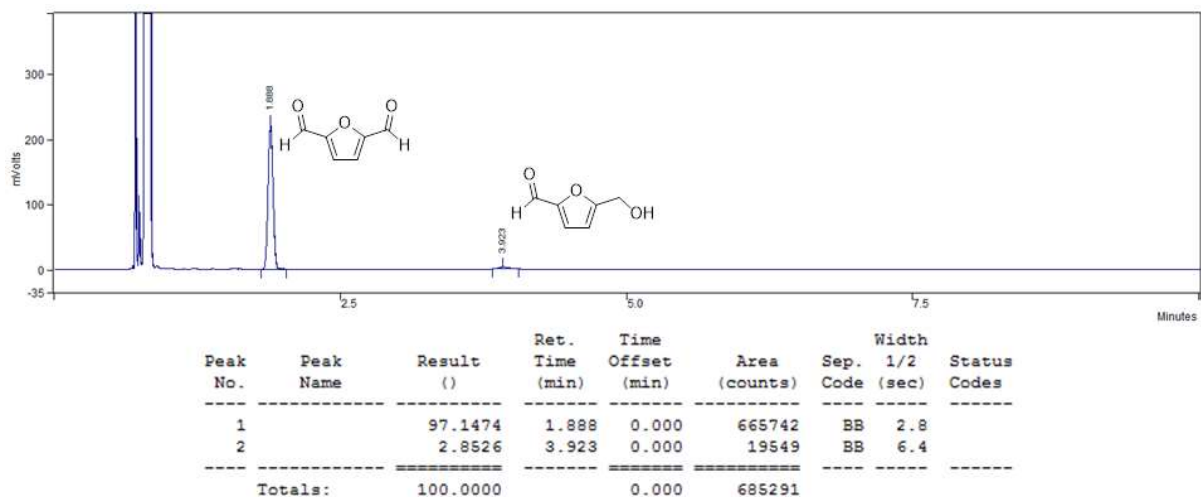


Figure S61. Gas chromatogram of 5-hydroxymethylfurfural (HMF) reaction (Table 4, Entry 18)

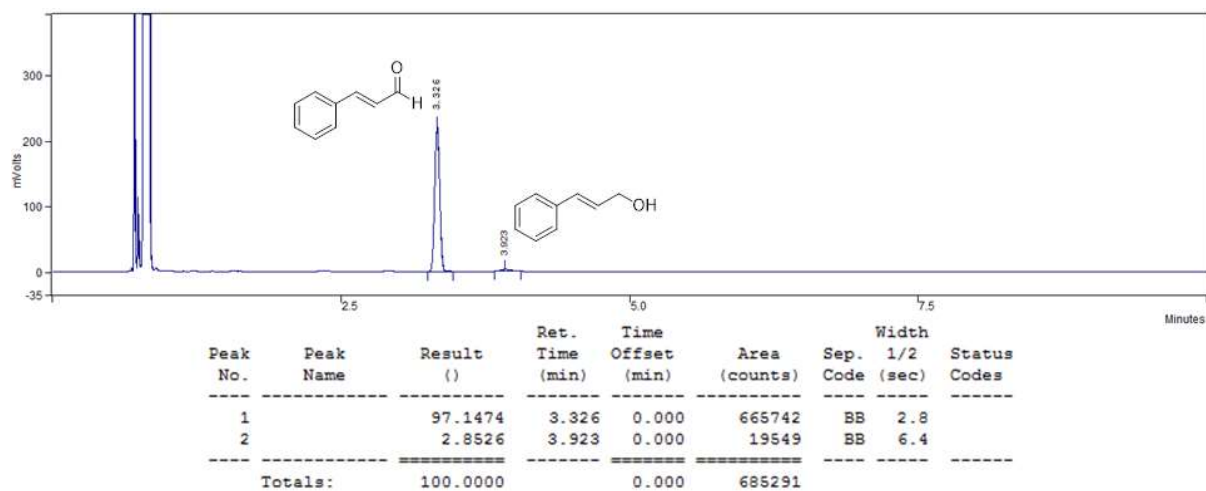


Figure S62. Gas chromatogram of cinnamyl alcohol reaction (Table 4, Entry 19)

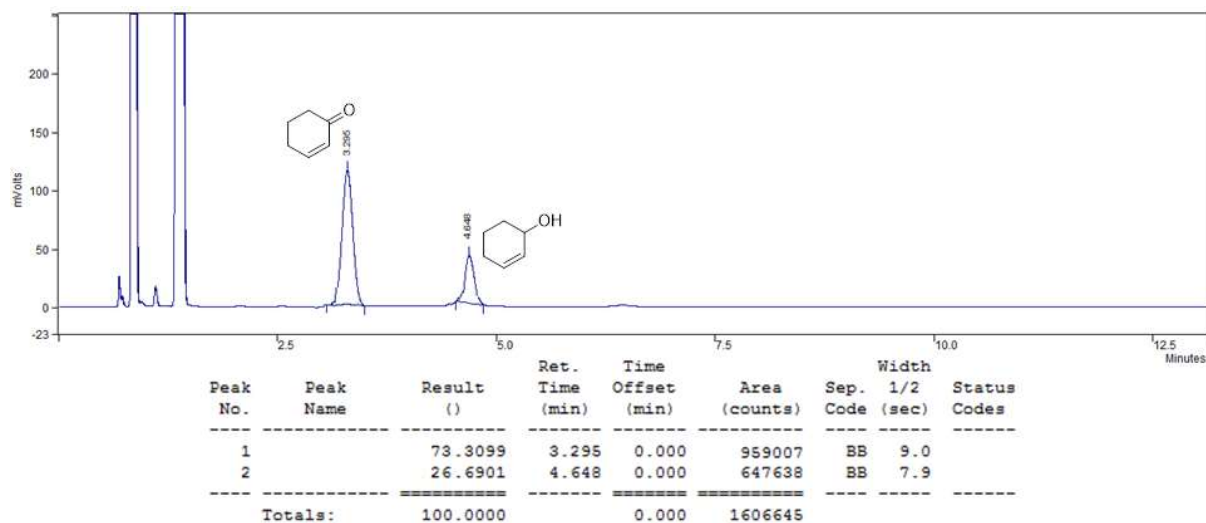


Figure S63. Gas chromatogram of 2-cyclohexene-1-ol reaction (Table 4, Entry 20)

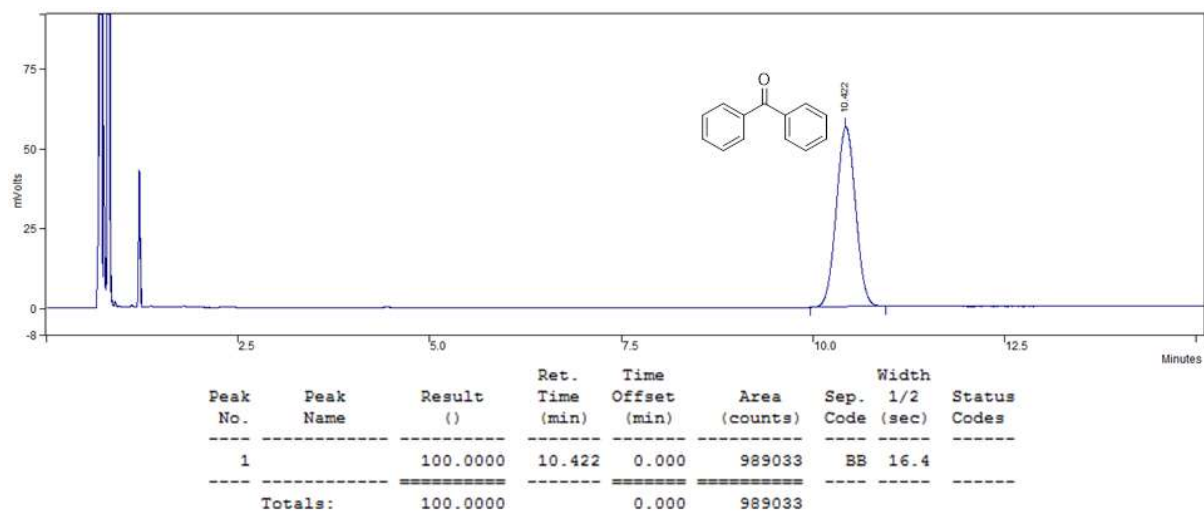


Figure S64. Gas chromatogram of diphenylmethanol reaction (Table 4, Entry 21)

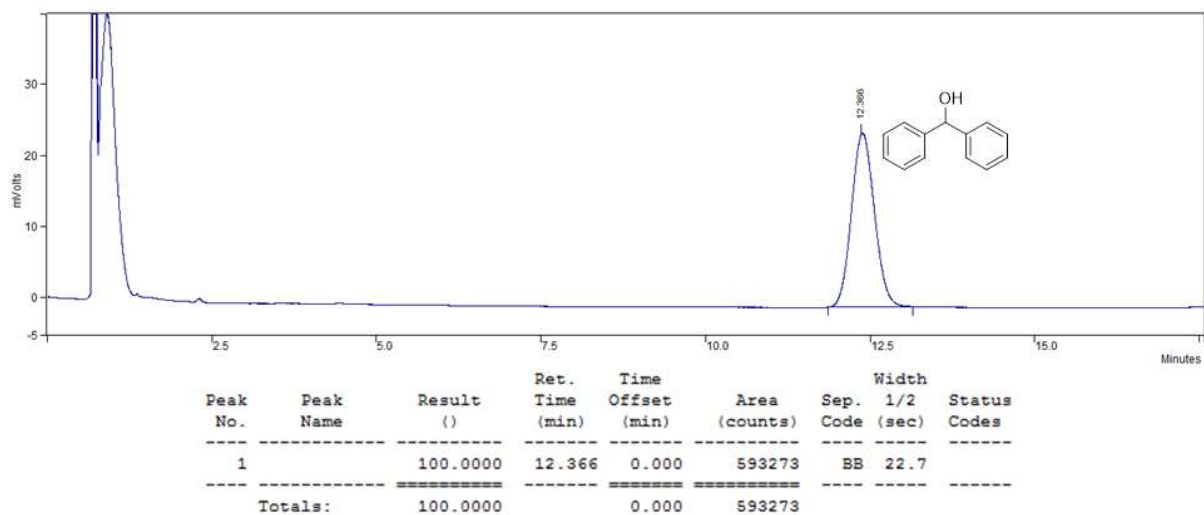


Figure S65. Gas chromatogram of diphenylmethanol (blank)

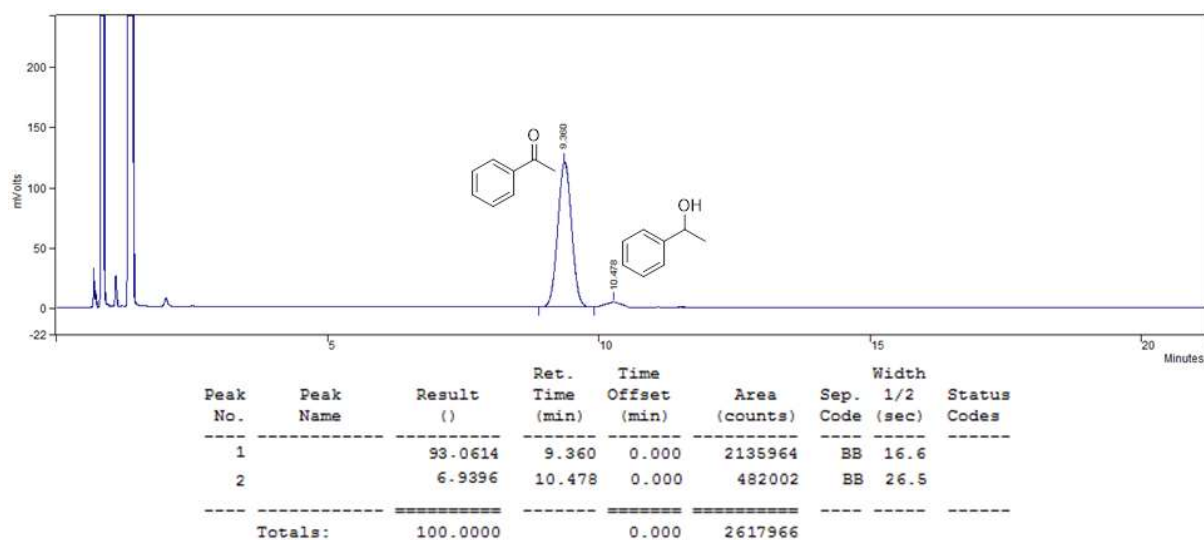


Figure S66. Gas chromatogram of 1-phenyl-1-ethanol reaction (Table 4 Entry 22)

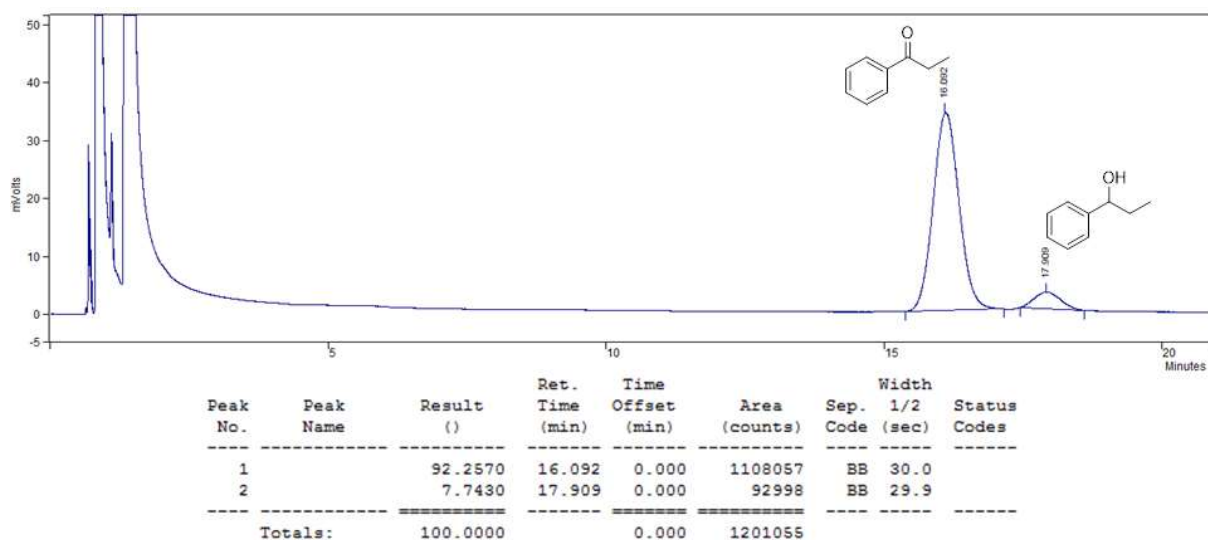


Figure S67. Gas chromatogram of 1-phenyl-1-propanol reaction (Table 4, Entry 23)

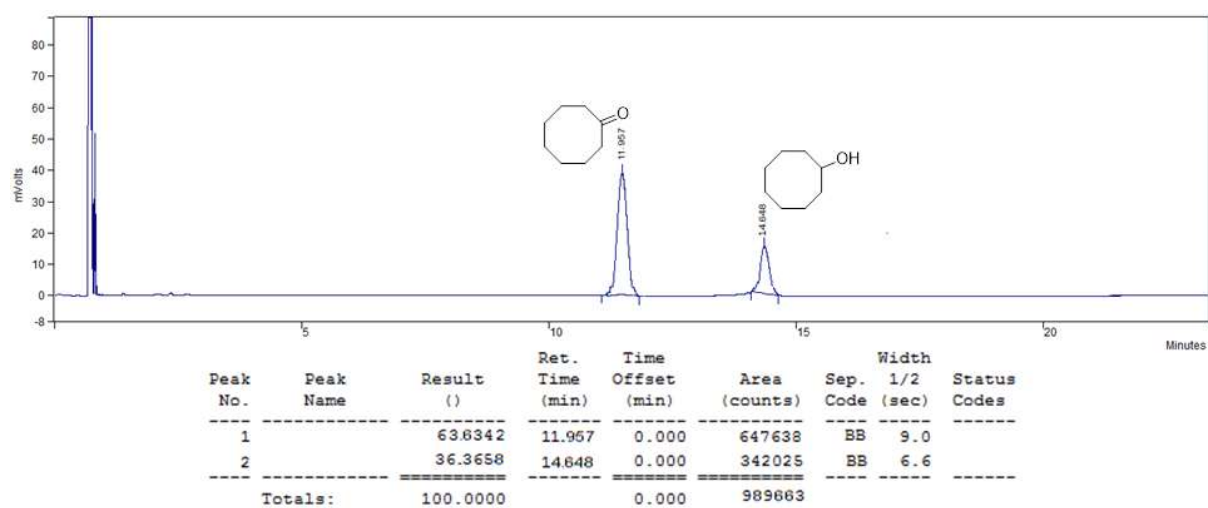


Figure S68. Gas chromatogram of cyclooctanol reaction (Table 4, Entry 24)

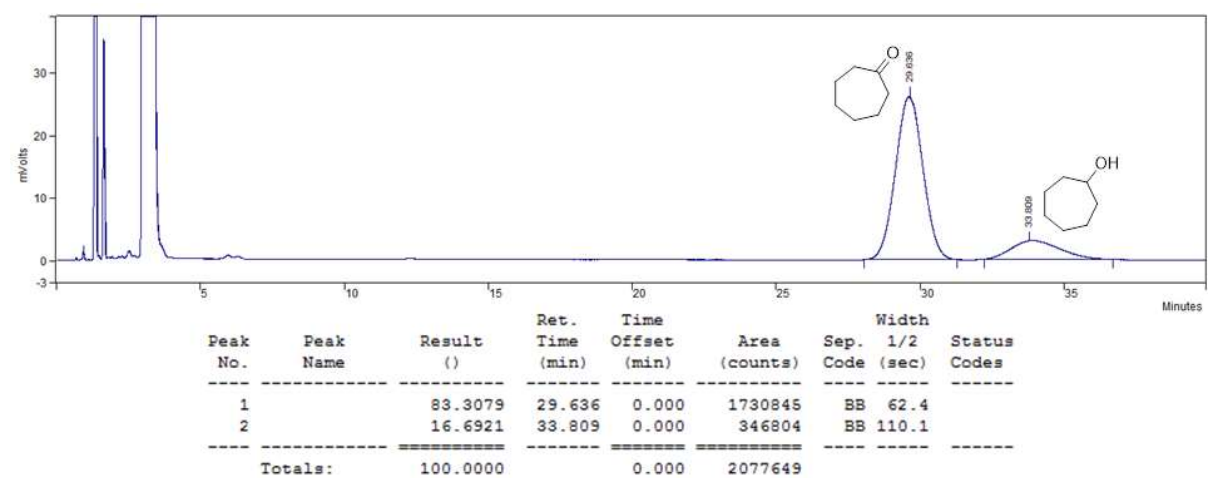


Figure S69. Gas chromatogram of cycloheptanol reaction (Table 4, Entry 25)

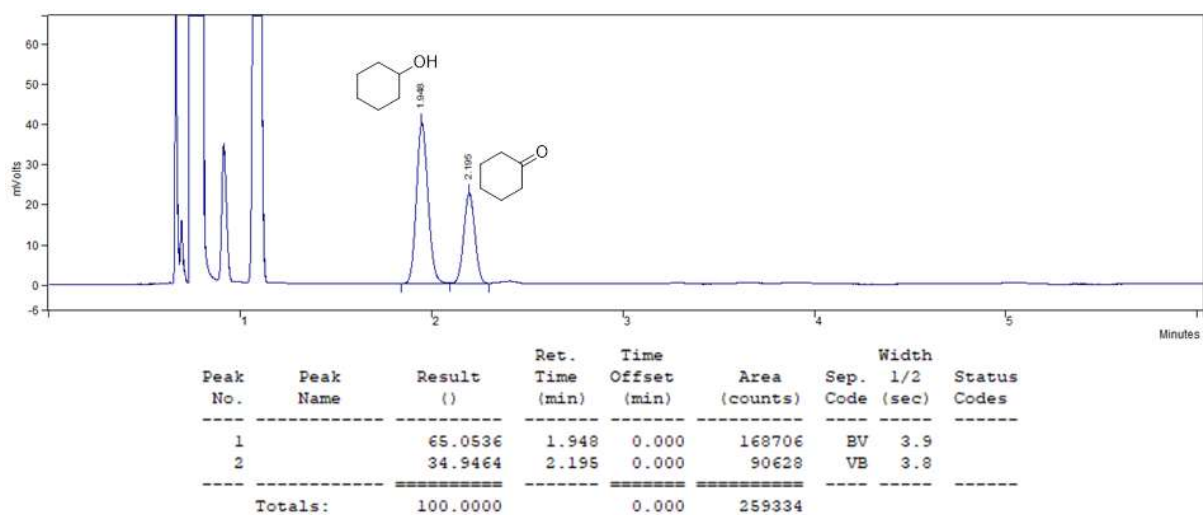


Figure S70. Gas chromatogram of cyclohexanol reaction (Table 4, Entry 26)

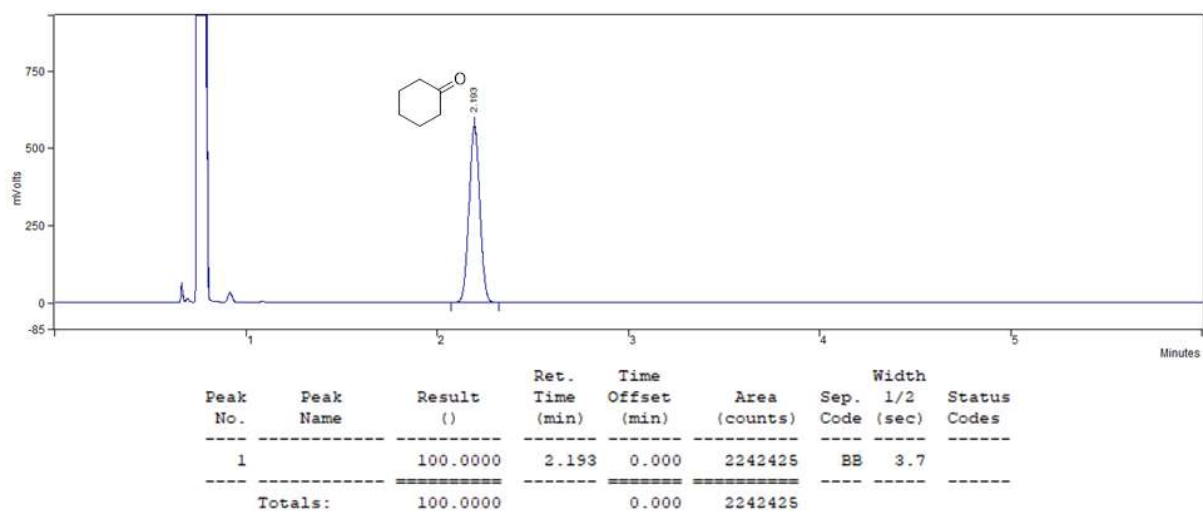


Figure S71. Gas chromatogram of cyclohexanone (blank)

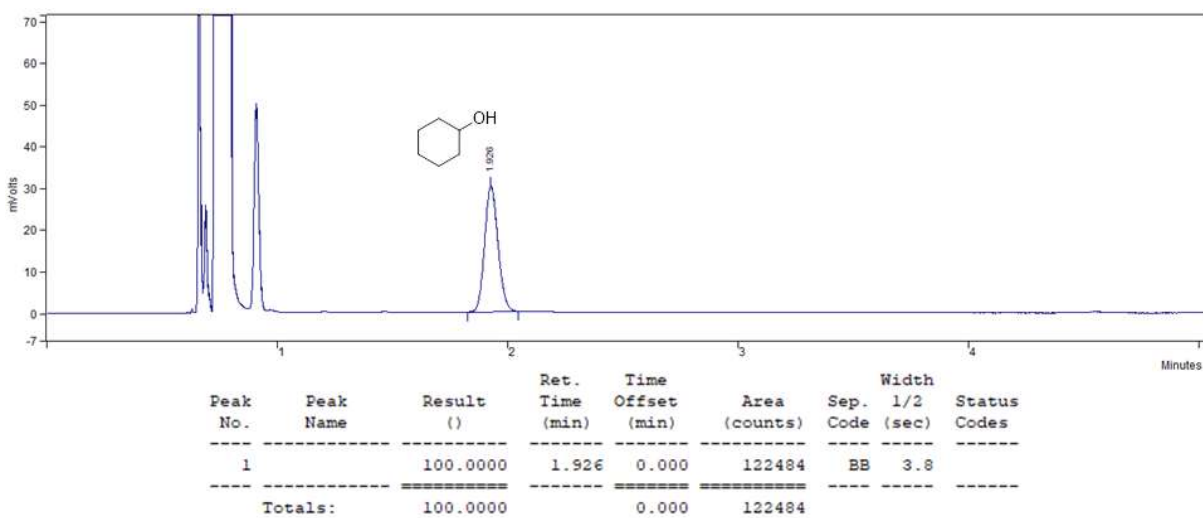


Figure S72. Gas chromatogram of cyclohexanol (blank)

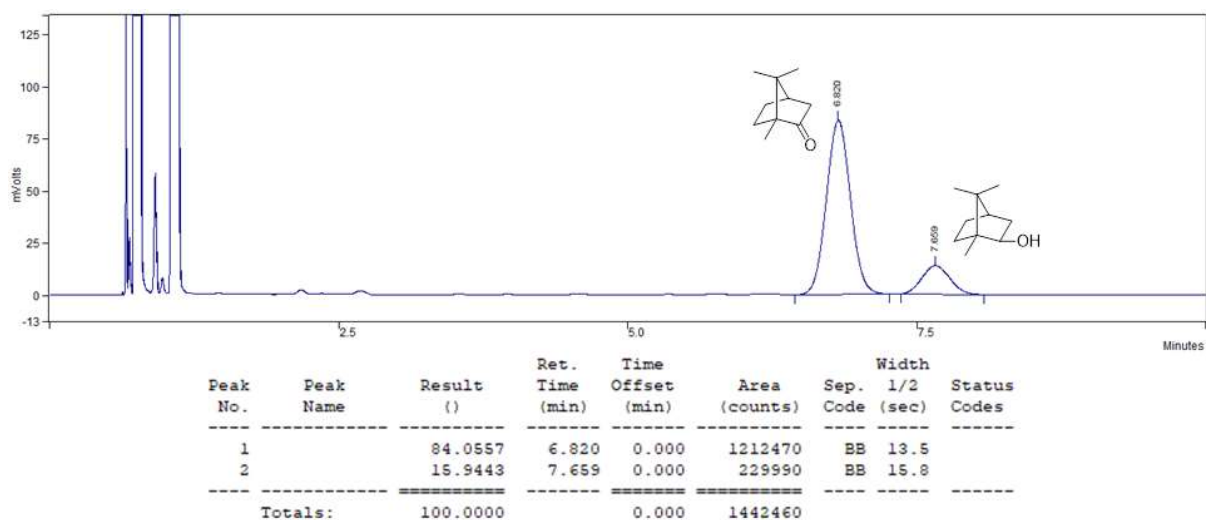


Figure S73. Gas chromatogram of borneol reaction (Table 4, Entry 27)

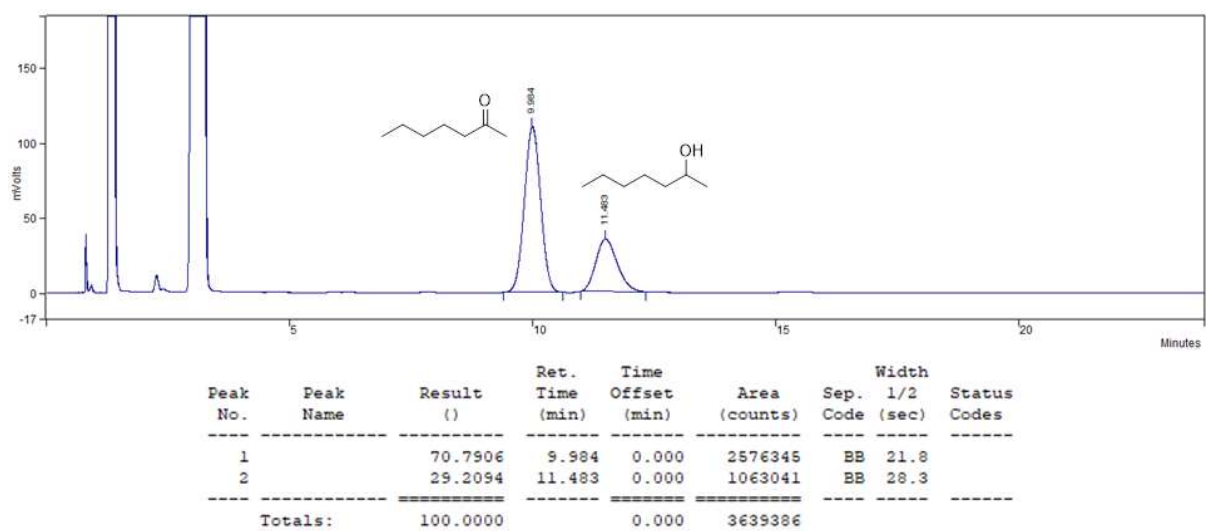


Figure S74. Gas chromatogram of 2-heptanol reaction (Table 4, Entry 28)

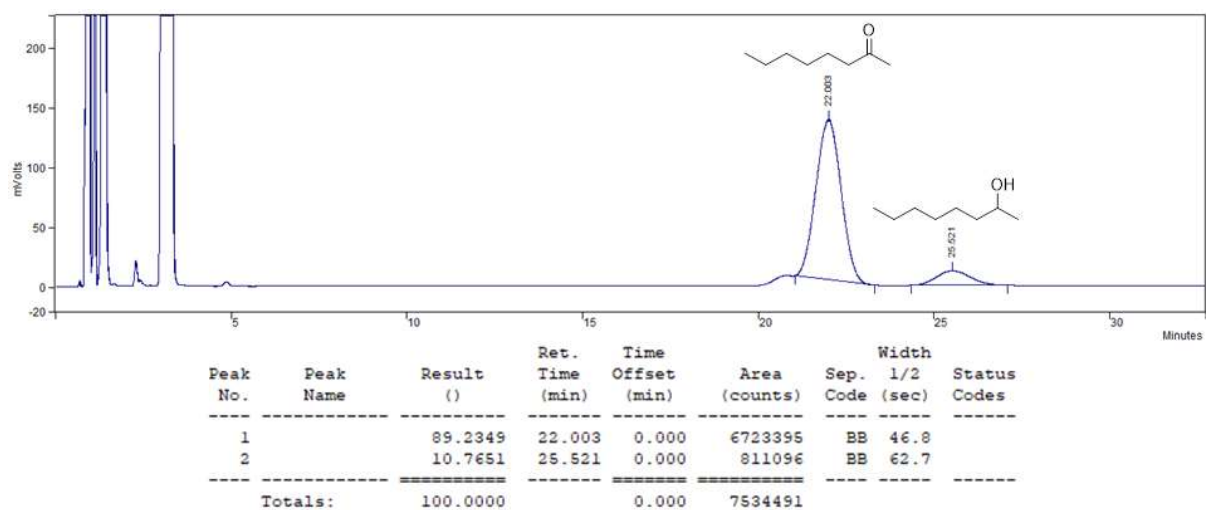


Figure S75. Gas chromatogram of 2-octanol reaction (Table 4, Entry 29)

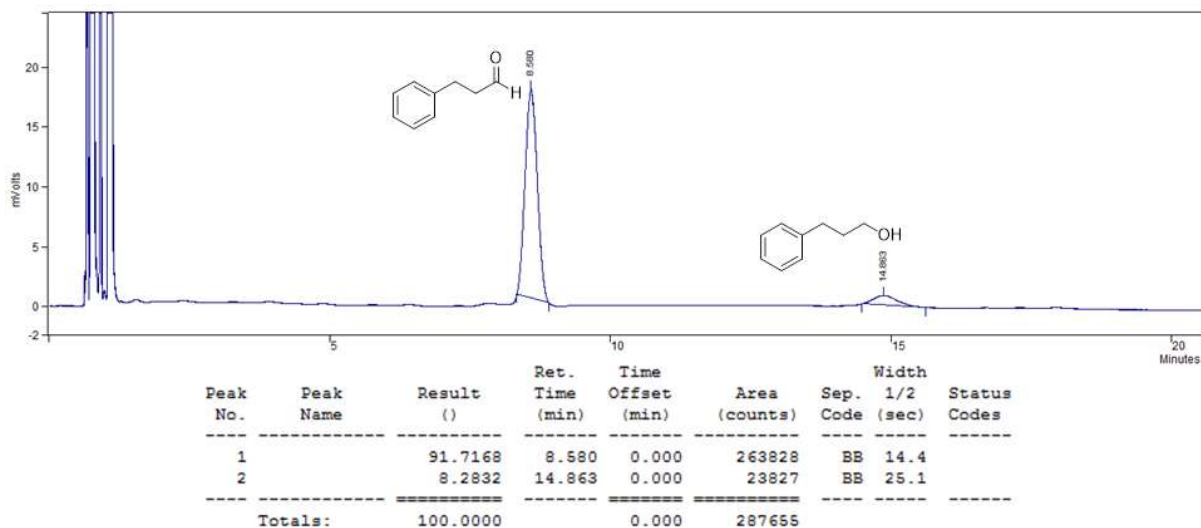


Figure S76. Gas chromatogram of 3-phenyl-1-propanol reaction (Table 4, Entry 30)

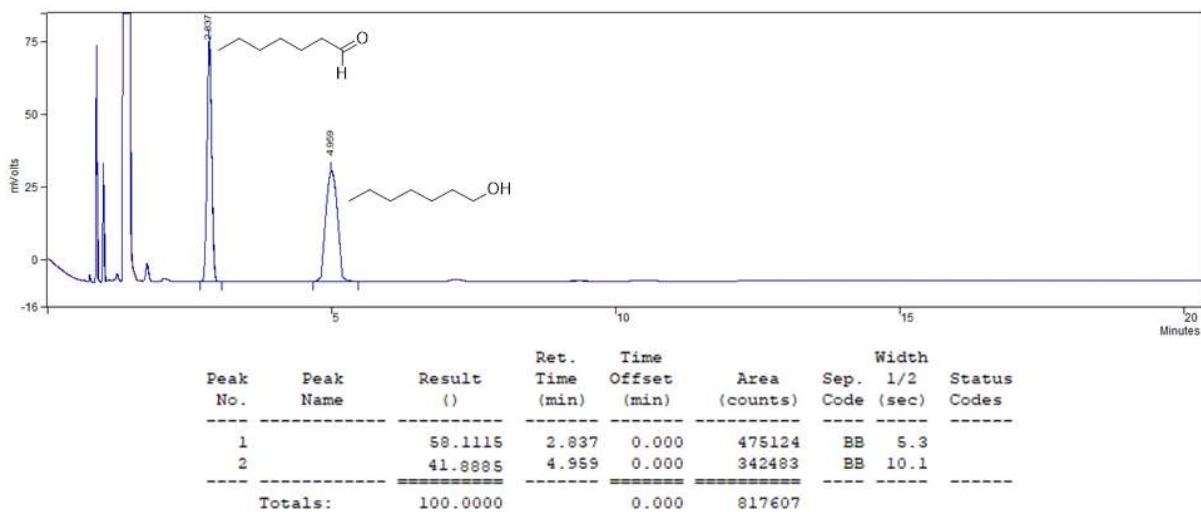


Figure S77. Gas chromatogram of 1-heptanol reaction (Table 4, Entry 31)

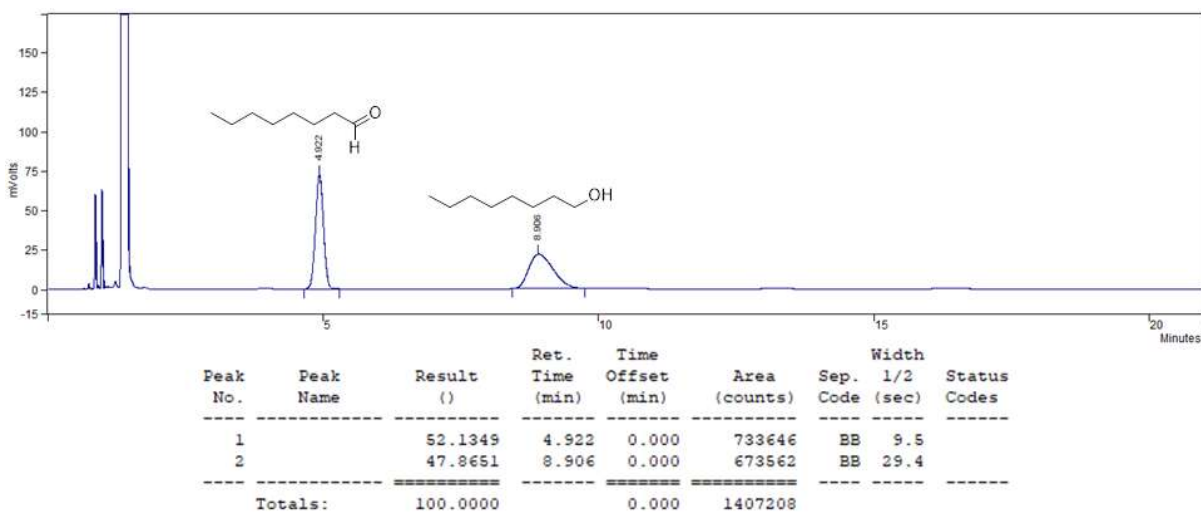


Figure S78. Gas chromatogram of 1-octanol reaction (Table 4, Entry 32)

- 1 B. Karimi, M. Khorasani, H. Vali and R. Luque, *J. Mater. Chem. A*, 2015, **3**, 6575.
- 2 B. Karimi, D. Elhamifar, O. Yari, M. Khorasani, H. Vali, J. H. Clark and A. J. Hunt, *Chem. Eur. J.*, 2012, **18**, 13520.
- 3 K. Yamaguchi and N. Mizuno, *Angew. Chem. Int. Ed.*, 2002, **41**, 4538.
- 4 V. V. Costa, M. J. Jacinto, L. M. Rossi, R. Landers and E. V. Gusevskaya, *J. Catal.*, 2011, **282**, 209.
- 5 M. R. Patil, A. R. Kapdi and A. Vijay Kumar, *ACS Sustain. Chem. Eng.*, 2018, **6**, 3264.
- 6 M. A. Hussain, M. Irshad, E. Ul Haq, S. Park, M. Atif, A. S. Hakeem, B. G. Choi and J. W. Kim, *Ind. Eng. Chem. Res.*, 2019, **58**, 23025.